INTERNAL OVERVOLTAGE PROTECTION OF DISTRIBUTION TRANSFORMERS

by

Thomas Owen Bialek, B. Sc. (EE)

A thesis
presented to the University of Manitoba
in partial fulfillment of the
requirements for the degree
Master of Science
in
Electrical Engineering

ISBN 0-315-34053-3

INTERNAL OVERVOLTAGE PROTECTION OF DISTRIBUTION TRANSFORMERS

BY

THOMAS OWEN BIALEK

A thesis submitted to the Faculty of Graduate Studies of
the University of Manitoba in partial fulfillment of the requirements
of the degree of

MASTER OF SCIENCE

I hereby declare that I am the sole author of this thesis.

I authorize the University of Manitoba to lend this thesis to other institutions or individuals for the purpose of scholarly research.

Thomas Owen Bialek

I further authorize the University of Manitoba to reproduce this thesis by photocopying or by other means, in total or in part, at the request of other institutions or individuals for the purpose of scholarly research.

Thomas Owen Bialek

The University of Manitoba requires the signature of all persons using or photocopying this thesis. Please sign below, and give address and date.

This thesis introduces the concept of under-oil arrestors to eliminate most of the conventional arrestor problem areas. Although a relatively new technology, this form of system protection offers improved arrestor-transformer assembly reliability.

The volt-ampere characteristics have been verified and low voltage surge testing has illustrated the feasibility of producing a smaller transformer by reducing the insulation required. Compatibility tests between the zinc oxide blocks and the transformer insulating system, performed during the course of this thesis and by arrestor manufacturers, have not demonstrated to date adverse effects on the performance of the blocks.

Although under-oil arrestors solve many of the problems with conventional arrestors, the main applications appear to be in salt fog or highly contaminated environments and underground distribution systems.

Acknowledgements

At this time the author would like to express his gratitude to the following people:

Brian Klaponski, Carte Electric

Dr. M.R. Raghuveer, University of Manitoba

Gord Toole, University of Manitoba

Dick Lode, Manitoba Hydro

Ron Mazur, Manitoba Hydro

Table of Contents

List of Figures

List of Tables

1. Introduction

1.1 Distribution Transformers

The role of a distribution transformer is to convert high system voltages, which are more economical for transferring energy over long distances, to a lower voltage which is more suitable for use by customers. Distribution class transformers provide an important link between the generation and consumption of power and are more plentiful than the transformers involved in power transmission.

Since a distribution transformer is a static device the reliability associated with it is very high; however, there is an abnormal failure rate. The main reasons for the occurrence of failure modes are overvoltages, long term overloads and manufacturing problems respectively.[1] At distribution class levels the most common form of overvoltage is generated by the occurrence of lightning discharges. By utilizing a lightning arrestor to limit the voltage appearing at the transformer terminals, the transformer is protected; a process known as insulation coordination.

1.2 Lightning Arrestors

In the past many types of lightning arrestors were designed and utilized.[4] Spark gaps have been used in many forms for the protection of power systems since the inception of overvoltage protection; however, gaps do not prevent the flow of the power follow-through current which results in a line-to-ground fault on the system. The introduction of current limiting resistors, such as electrolytic and oxide film resistor, improved the performance of the gaps as arrestors. Silicon Carbide, SiC, gapped arrestors were developed next and are still utilized in hydro installations throughout the world today. In 1968 the Matsushita Electric Industrial Co. in Japan developed low voltage gapless surge protection devices based on a Zinc Oxide, ZnO, non-linear resistor. The development of this device is still continuing; at the present time the Matsushita company licenses the technology for lightning arrestors at the distribution, intermediate and station class level based on ZnO valve blocks.

An ideal arrestor has the volt-ampere characteristics shown in Figure 1. The device does not conduct current until a certain voltage is reached; the value of 1.43 per unit coincides with the ZnO at 10 amperes. Once this voltage level is reached on the system, the arrestor conducts and limits any further voltage increase. Figure 1 also illustrates the volt-ampere characteristics of both a Silicon Carbide, SiC, and Zinc Oxide,

ZnO, arrestor. Obviously the performance of the ZnO arrestor models the ideal arrestor more closely than a comparable SiC unit.

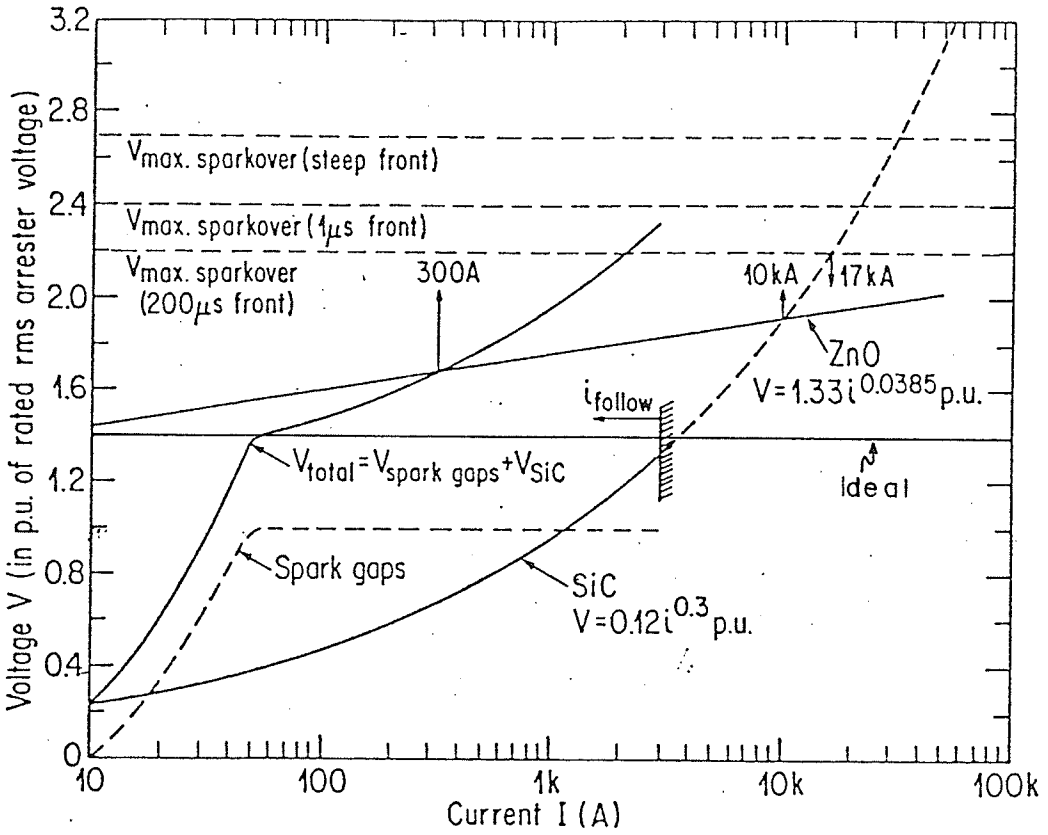

Figure 1 Volt-Ampere Characteristics of an Ideal, SiC and ZnO Arrestor [24]

1.2.1 Zinc Oxide Versus Silicon Carbide

By comparing a SiC and similar gapless ZnO arrestor it is possible to list the following advantages of a ZnO arrestor.

1) There are no series gaps which means smoother transition into the conduction mode of the arrestor.
2) There is no power follow through current once the arrestor operates.

3) Zinc Oxide arrestors have lower impulse current discharge voltages.

4) As the impulse current front time decreases, the discharge voltage levels increase more slowly than for a SiC arrestor.

5) Internal heating of a ZnO block does not affect the impulse current discharge voltage levels while SiC blocks are affected.

6) The arrestor complexity is reduced resulting in increased reliability since there are no series gaps.

7) A ZnO arrestor is less susceptible to the effects of contamination since there are no internal gap grading problems.

8) A Zinc Oxide arrestor has better overload capabilities.

9) There is also a higher degree of non-linearity with ZnO arrestors.

Obviously, ZnO arrestors should be the natural choice for most protective applications.

1.2.2 Current Overvoltage Protection Problems

However there are problems with the current state of the art in transformer protection as listed below:

1) arrestor housing contamination from either accumulated dirt or salt spray,

2) animals such as squirrels and birds causing outages by connecting the line to ground,

3) vandalism,

4) moisture ingress in the arrestor housing,

5) inductive voltage produced in the arrestor lead length,

6) lowered protective margins due to equipment ageing.

The most pressing problem is the lowered protective margins and a more detailed discussion is necessary.

American National Standards Institute, ANSI C62.2-1981, recommends a protective margin of at least 20% for transformers.[2] The protective margin is described by Equation 1 where the discharge voltage is due to an 8 x 20 microsecond, 10 kiloampere current surge. In overhead distribution applications

$$\% \text{ protective margin} = \frac{\text{BIL - discharge voltage level}}{\text{discharge voltage level}} \times 100 \qquad 1)$$

Silicon Carbide arrestors provide adequate margins; however, the actual protective margin may be lower than the calculated protective margin for the following reasons. As a transformer ages, the basic impulse insulation level, BIL, of the unit also decreases; a 20% reduction of the initial BIL level of the unit has been suggested. It is also generally accepted that 30% of all impulse current front times are less than 1 microsecond and 95% of all lightning strokes have a current magnitude greater than 14 kiloamps.[4] Finally, there is the effect of arrestor lead length on its protective level; conservative estimates are 1.2 kilovolts

per foot of lead length. All these factors contribute to a lowered protective margin.

For open tie, underground distribution systems protected by an arrestor at the riser pole only, shown in Figure 2, the protective margins with SiC arrestors are marginal. This is due to the fact that the reflected wave at the open termination is in phase with the incoming wave; as a consequence, voltage doubling of the waveform occurs. Table 1 further illustrates the differences between protective margins calculated for a 13.2 kV system with and without lead lengths and a faster rate of rise with an arrestor located at the riser pole only. In Table 1 the following abbreviations are used: BIL equals basic impulse level, FOW is front of wave determined by a 10 kiloamp wave cresting in 0.5 microsecond, 10 kA IR is the 10 kiloamp discharge voltage, CW is chopped wave and ROR is rate of rise. The standard rate of rise referred to is an 8 X 20 microsecond waveform and the comparisons are made for a SiC, DA-IV 10; ZnO, DV-8.4; and ZnO heavy duty, VR-8.4, distribution class arrestors. The initial entry for each type of arrestor is the calculation shown in Equation 1 and neglects any possible reduction in BIL levels. For example the BIL Percent Margin for the SiC arrestor row 1 column 10, is calculated as follows with all the values being obtained from row 1.

column 10 = (column 3 - column 8)/ column 8 x 100

32=(95 - 72)/ 72 x 100

Also the Chopped Wave Percent Margin, row 1 column 9, can be obtained as follows and again all values are listed in row 1.

column 9 = (column 2 - column 7)/ column 7 x 100

22=(110 - 90)/ 90 x 100

The Percent Margin values for the remaining row can be calculated by the same methodology. Each additional entry in the table illustrates a progressively worsening scenario. It is obvious that eventually all protective margins will be either unacceptable or marginal for any type of distribution class arrestor due to the previously mentioned factors. By observing Table 2, which conveys information similar to that contained in Table 1 for a 24 kV system, it is apparent that the protective margins are lower and unacceptable for the Equation 1 calculation. For a four foot lead length and three times faster rate of rise all protective margins are negative for any type of distribution class arrestor. At this point it is obvious that an arrestor at the riser pole is inadequate and an additional arrestor is required at the open tie. Table 3 pertains to a 34.5 kV system with an arrestor at the riser pole and the open tie. However at this system voltage the protective margins again become marginal or unacceptable. Including the effects of ageing only worsens the calculated margins. The only solution to this problem is to employ arrestors at the riser pole, open tie and at every transformer.

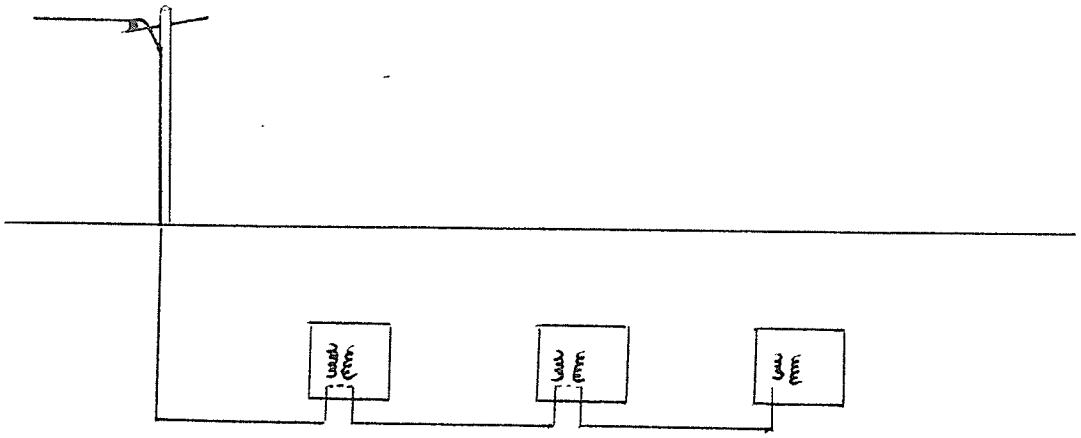

Figure 2 Open Tie, Underground Distribution System

System Voltage	Insulation CW	Insulation BIL	Arrester and Lead Data Type	FOW	10-kA IR	Voltage Doubling (2) FOW	Voltage Doubling (2) 10-kA IR	Percent Margin CW	Percent Margin BIL	Type of Protection
13.2	110	95	DA-IV 10	45	36	90	72	22	32	No Lead Standard ROR
13.2	110	95	DA-IV 10	45	42.5	90	85	22	12	4' Lead Standard ROR
13.2	110	95	DA-IV 10	69	56	138	112	−20	−15	4' Lead 3 Times Faster ROR
13.2	110	95	DV-8.4	36.5	32	73	64	51	48	No Lead Standard ROR
13.2	110	95	DV-8.4	42.5	38.5	85	77	29	23	4' Lead Standard ROR
13.2	110	95	DV-8.4	54	48	108	96	2	0	4' Lead 3 Times Faster ROR
13.2	110	95	VR-8.4	33.5	29	67	58	64	64	No Lead Standard ROR
13.2	110	95	VR-8.4	40	35.5	80	71	37	34	4' Lead Standard ROR
13.2	110	95	VR-8.4	50	45	100	90	10	6	4' Lead 3 Times Faster ROR

Table 1 Examination of Underground Insulation Protective Margins with Arrestor at Riser Pole Only - 13.2 kV System [31]

System Voltage	Insulation CW	Insulation BIL	Arrester and Lead Data Type	FOW	10-kA IR	Voltage Doubling (2) FOW	Voltage Doubling (2) 10-kA IR	Percent Margin CW	Percent Margin BIL	Type of Protection
24.9	145	125	DA-IV 18	87	67	174	134	−17	−7	No Lead Standard ROR
24.9	145	125	DA-IV 18	93	73.5	186	147	−22	−15	4' Lead Standard ROR
24.9	145	125	DA-IV 18	113	93	226	186	−36	−33	4' Lead 3 Times Faster ROR
24.9	145	125	DV-15.3	66.5	59	134	118	8	6	No Lead Standard ROR
24.9	145	125	DV-15.3	72.5	65	146	130	0	−4	4' Lead Standard ROR
24.9	145	125	DV-15.3	87	77	174	154	−17	−19	4' Lead 3 Times Faster ROR
24.9	145	125	VR-15.3	61	52	122	104	19	20	No Lead Standard ROR
24.9	145	125	VR-15.3	67	58.5	134	117	8	7	4' Lead Standard ROR
24.9	145	125	VR-15.3	80	70	160	140	−9	−11	4' Lead 3 Times Faster ROR

Table 2 Examination of Underground Insulation Protective Margins with Arrestor at Riser Pole Only - 24.9 kV System [31]

System Voltage	Insulation BIL	Arrester and Lead Data Type	FOW	10-kA IR	Maximum Cable Voltage	Percent Margin BIL	Type of Protection
34.5	150	DA-IV 27	79	96	136*	10	No Lead Standard ROR
34.5	150	DA-IV 27	79	102	142*	6	4' Lead Standard ROR
34.5	150	DA-IV 27	79	128	168*	−11	4' Lead 3 Times Faster ROR
34.5	150	DV-22	97	86	115**	30	No Lead Standard ROR
34.5	150	DV-22	97	92	121**	24	4' Lead Standard ROR
34.5	150	DV-22	97	107	136**	10	4' Lead 3 Times Faster ROR
34.5	150	VR-22	88	76	102**	47	No Lead Standard ROR
34.5	150	VR-22	88	82	108**	39	4' Lead Standard ROR
34.5	150	VR-22	88	97	123**	22	4' Lead 3 Times Faster ROR

*IR of riser arrester plus ½ sparkover of open-tie arrester.
**IR of riser arrester plus a reflected wave of 26 kV for VR and 29 kV for DV; from computer simulation.

Table 3 Examination of Underground Insulation Protective Margins with Arrestor at Riser Pole and at Open Tie - 34.5 kV System [31]

The reduced protective margins are one of several problems that are associated with underground distribution systems. Another major problem is the adverse effect of severe lightning discharges on cable life. Although utilities expect a service life of thirty years for underground cables, in some cases, due to the cumulative effect of overvoltages, cables have failed within three years. Generally cable replacement is complicated and expensive; it is more economical to provide overvoltage protection at each transformer. Therefore, for underground distribution systems, it is necessary for the distribution engineer to seriously consider the advantages of under-oil protection.

1.2.3 Solution To Arrestor Problems

A solution to most conventional problems with arrestors, listed in Section 1.2.2 is the ZnO under-oil arrestor. By placing the arrestor inside the tank, the arrestor-transformer assembly offers greater reliability, improved unit life, cost savings in the form of decreased outage rate and greater protective margins. Further benefits of ZnO under-oil arrestors are possible; one United States utility employs under-oil arrestors in all distribution transformer applications and claims a thousand to one improvement in arrestor related failures over a Silicon Carbide unit of the same rating.

1.3 Zinc Oxide Under-Oil Arrestors

There is a chemical reaction between uncoated blocks and the oil. This reaction leaves a zinc coating on the outside of the blocks. Once a few thousandths of an inch are machined off the outside of the blocks, the performance of the blocks returns to normal levels. The chemical reaction does not debase the oil. All under-oil arrestor manufacturers have eliminated this problem by coating the blocks with a proprietary material which prevents the chemical reaction; resulting in a block which is impervious to oil.

One of the major concerns with under-oil arrestors is the high ambient temperatures which could lead to possible thermal runaway.[25] However, it has been found that the surge discharge characteristics are unaffected by the ambient temperatures. Only the normal leakage currents are temperature sensitive and with proper design techniques thermal runaway can be avoided. Oil is superior to air as a heat transfer medium and allows the ZnO blocks to operate under higher temporary overvoltages. Ohio Brass, an under-oil arrestor manufacturer, provides longer zinc oxide blocks to lower the leakage currents and the risk of thermal runaway. The extra material adds only slightly to the impulse current discharge voltage level, but this increase is offset by the fact that lead lengths in this application are negligible. Both General Electric and Ohio Brass suggest fusing

the arrestor to prevent excessive power frequency overvoltage currents through the arrestor which can lead to arrestor failure. However, if circuit breakers are coordinated properly the need for fusing can be eliminated.

1.4 Thesis Objectives

One of the original objectives of this thesis was to develop an under-oil arrestor assembly for any given transformer rating; however, once work was underway it became apparent that several leading United States manufacturers had already developed such a form of internal overvoltage protection. Rather than expend much time and effort it was decided to utilize currently available technology. Both Ohio Brass and General Electric offer similar under-oil arrestor assemblies, with the ZnO blocks housed in an eighth of an inch thick phenolic tube. Both end s of the tubing are open, allowing oil to circulate freely over the ZnO blocks. The blocks are held in place by a spring-aluminum terminal arrangement, which is quite similar to the porcelain arrestor assembly. This arrangement is compatible with the oil environment in which it is placed. Neither manufacturer utilizes series gaps; therefore oil decomposition due to arcing is eliminated.

1.5 Currently Available Designs

General Electric offers a "fail open" under-oil arrestor while Ohio Brass offers a "fail closed" design. "Fail open" means that the arrestor fails as an open circuit. Since the manufacturer has provided a weakened point near the top terminal, when the phenolic housing is ruptured by the mechanical stresses produced as the ZnO blocks shatter the blocks are able to drop to the bottom of the tank. Exact details of the weakening method are proprietary. The advantage of this system is that the transformer can continue to operate although unprotected against future overvoltages but the biggest disadvantage is the lack of suitable means of detecting a failed under-oil arrestor. On the other hand, the "fail closed" design presents the system with a line-to-ground fault. The failed ZnO blocks are contained within the phenolic housing preventing Zinc Oxide particles from falling into the transformer coils. The main advantage of this system is that the failed arrestor can be detected and located by closing in on the fault in the system; however, the fault within the transformer can not be cleared until the transformer is removed from the system.

Although there are some problems associated with under-oil arrestors, Such a method of protection is still superior to mounting an arrestor externally next to the high voltage bushing. As previously mentioned some of the main advantages of under-oil

arrestors are in the areas of contamination, vandalism, improved thermal capabilities and negligible lead lengths.

2. Zinc Oxide Blocks

2.1 Physics of Zinc Oxide Blocks

Zinc Oxide arrestors are a complex combination of various compounds, with Zinc Oxide accounting for approximately 90% of the total material in a block. However, a small change in the quantities of other materials plays an important role in the final performance of the arrestor blocks. A typical idealized microstructure picture of a ZnO block is shown in Figure 3B, while the actual microstructure is shown in Figure 3A. The initial low leakage current is due to capacitive conduction between the ZnO grains; however, as the voltage gradient in the block is increased the resistive component of current also increases. Once the current through the ZnO block exceeds a milliamp the current is entirely resistive. A more detailed discussion of the actual conduction mechanisms in zinc oxide blocks can be found in Appendix 1. A brief description of the ZnO block manufacturing process has been included in Appendix 2.

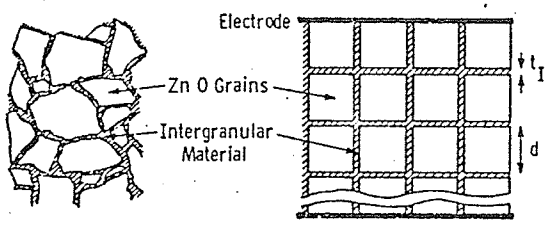

A) Typical B) Ideal

Figure 3 Zinc Oxide Microstructure

2.2 Volt-Ampere Characteristics

To determine the volt-ampere characteristics of the zinc oxide blocks, several tests were performed. It is well known that the ZnO block's volt-ampere relation is in the form of a power relationship, Equation 2. The validity of this relation was confirmed under AC, DC, impulse voltage and current waveforms.

$$I=aV^{b} \qquad 2)$$

2.2.1 DC Volt-Ampere Characteristics

The DC volt-ampere characteristics were determined using the test arrangement shown in Figure 4. Unfortunately, the limited energy capabilities of the supply prevented the experimental determination of the volt-ampere characteristics at large current magnitudes. The test results are shown in Table 4. It is interesting to note that the current flow was initiated once the voltage reached the maximum continuous operating voltage of the blocks submitted to the applied voltage. Also, the onset of conduction is a function of the number of ZnO blocks in series within the assembly; that is two and three blocks start conducting current at approximately two and three times the starting voltage level of one block. This is an indication of the uniformity of the manufacturing process since two blocks have twice the number of grains and boundaries; the critical gradient is therefore double the value for one block. As well it

illustrates the resistive nature of the current in the highly non-linear region since until a critical voltage level is obtained there is no current flow which would be associated the capacitive coupling between the ZnO grains.

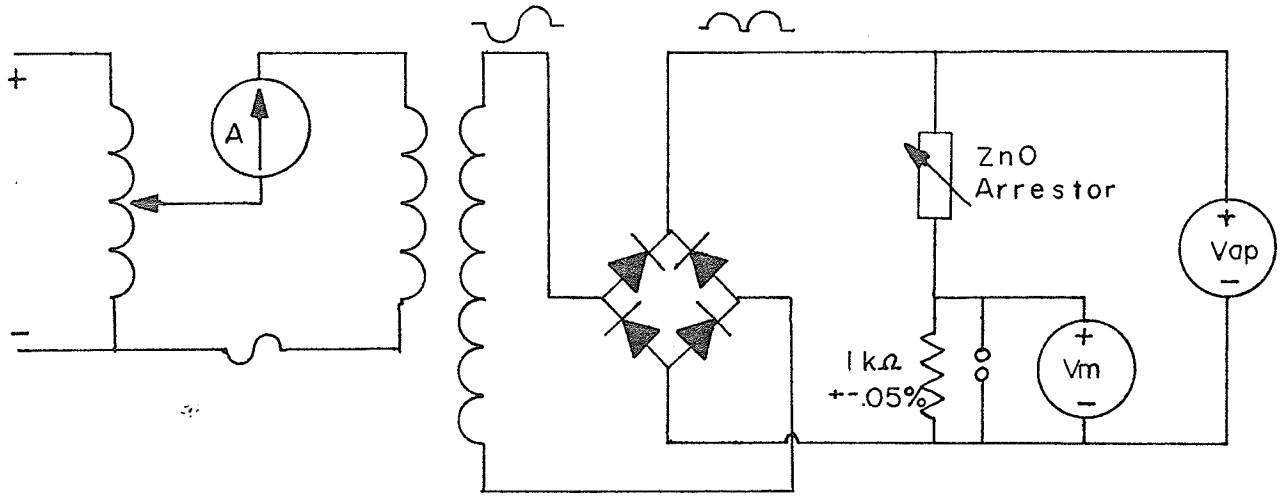

Figure 4 DC Volt-Ampere Characteristics Test Arrangement

Manufacturer 1						Manufacturer 2	
1 block		2 blocks		3 blocks		3 blocks	
Vap	Im	Vap	Im	Vap	Im	Vap	Im
0-2.5	0	0-6.5	0	0-9.0	0	0-13	0
3.0	.0002	7.0	.0003	9.5	.0003	14.0	.0002
3.5	.0035	7.5	.0007	10.0	.0005	14.5	.0003
4.0	.0208	8.0	.0014	10.5	.0008	15.0	.0004
4.5	.1240	8.5	.0096	11.0	.0013	15.5	.0006
4.6	.1720	9.0	.0147	11.5	.0020	16.0	.0010
4.7	.3100	9.5	.0242	12.0	.0030	16.5	.0017
4.8	.6534	10.0	.0291	12.5	.0047	17.0	.0036
4.9	1.510	10.5	.1060	13.0	.0068	17.5	.0080
		11.0	.6200	13.5	.0102	18.0	.0265
		11.2	1.130	14.0	.0157	18.5	.1330
				14.5	.0219	19.0	1.610
				15.0	.0413		
Vap is in kilovolts				15.5	.0646		
				16.0	.1087		
Im is in milliamps				16.5	.2032		
				17.0	.4043		
				17.5	.9032		
				18.0	1.951		

Table 4 DC Volt-Ampere Characteristics Test Values

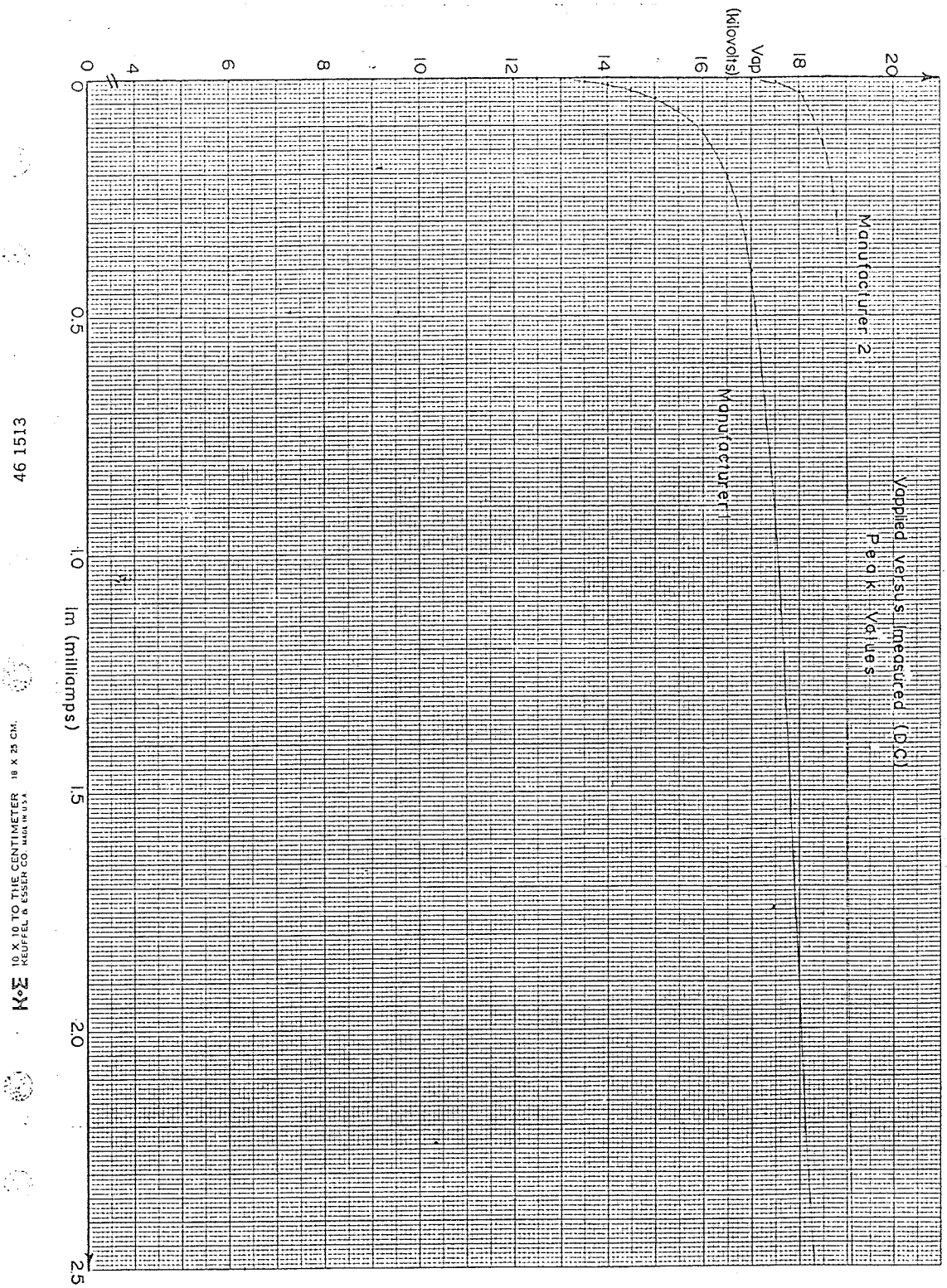

Figure 5 Plots of the DC Volt-Ampere Characteristics

The DC volt-ampere characteristics were determined for two different arrestor manufacturers' makes of blocks and the plots are shown in Figure 5. There is a slight difference between the two curves. This disparity is due to the different compound formulations used by the manufacturers and also the size variation of blocks. Although Matsushita licenses all manufacturers, they are free to experiment with the proportions of the compounds which make up a Zinc Oxide block.

A curve fitting program based on the least squares method was used to derive the value of b in Equation 2. For manufacturer 1, the value of b was found to be approximately 16 while for manufacturer 2 b was found to be approximately 26. Most papers cite the value of b in the range of 30-50; however, this value is valid for the highly non-linear portion of the volt-ampere curve which was unfortunately unobtainable with equipment available at the University of Manitoba. Only values in the leakage current and onset of conduction range were obtainable.

2.2.2 AC Volt-Ampere Characteristics

Next the volt-ampere characteristics were determined under ac excitation. Again two makes of ZnO blocks were tested by assembling the circuit shown in Figure 6. The results shown in Table 5 and plotted in Figure 7 show that the initial leakage currents in the Zinc Oxide blocks are capacitive in nature and

are due to the capacitance between the ZnO grains within the blocks. By comparing Figure 7 with 5 one observes that the resistive component of current predominates in the highly non-linear portion of the volt-ampere characteristics since both curves are identical after a few milliamps. Eventually the capacitive component of current ceases to exist.

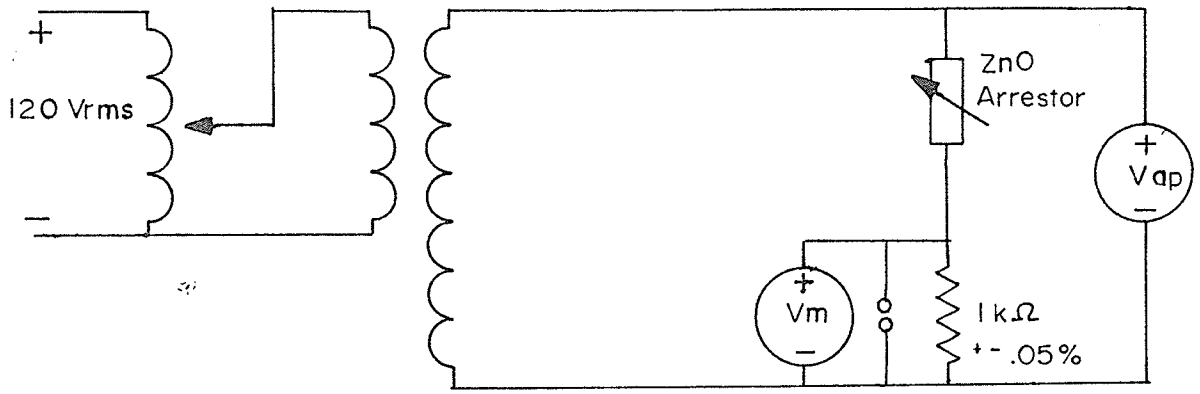

Figure 6 AC Volt-Ampere Characteristics Test Arrangement

Figure 7 again illustrates the difference in block formulations. As well it can be observed that the effects of blocks in series add linearly; meaning that the current through one block is approximately three times the current for three blocks at a set voltage level. This essentially means that the manufacturing process produces uniform blocks.

Again the value of b in Equation 2 was found for the different types of blocks. For manufacturer 1 the value, found by the least squares method, was approximately 14 while for manufacturer 2 this value was calculated to be 22. The AC supply was again the determining factor in the calculated values since

the energy requirements to obtain points in the highly nonlinear portion of the curve are large.

Manufacturer 1						Manufacturer 2	
1 block		2 blocks		3 blocks		3 blocks	
Vap	Im	Vap	Im	Vap	Im	Vap	Im
0.5	.0610	0.5	.0280	0.5	.0144	0.5	.0183
1.0	.1160	1.0	.0570	1.0	.0322	1.0	.0399
1.5	.1750	1.5	.0900	1.5	.0506	1.5	.0606
2.0	.2360	2.0	.1180	2.0	.0689	2.0	.0822
2.5	.3090	2.5	.1500	2.5	.0889	2.5	.1035
3.0	.3920	3.0	.1810	3.0	.1067	3.0	.1249
3.5	.5530	3.5	.2110	3.5	.1263	3.5	.1465
4.0	6.000	4.0	.2420	4.0	.1459	4.0	.1681
		4.5	.2700	4.5	.1640	4.5	.1883
		5.0	.3030	5.0	.1849	5.0	.2111
		5.5	.3350	5.5	.2027	5.5	.2308
		6.0	.3670	6.0	.2249	6.0	.2525
		6.5	.4030	6.5	.2412	6.5	.2726
		7.0	.4580	7.0	.2614	7.0	.2956
		7.5	.5440	7.5	.2833	7.5	.3160
		8.0	.8250	8.0	.3032	8.0	.3361
		8.5	5.921	8.5	.3228	8.5	.3553
				9.0	.3448	9.0	.3777
				9.5	.3670	9.5	.3956
				10.0	.3922	10.0	.4172
				10.5	.4207	10.5	.4372
Vap is in kilovolts RMS				11.0	.4536	11.0	.4576
				11.5	.4954	11.5	.4800
Im is in milliamps RMS				12.0	.5584	12.0	.5016
				12.5	.6949	12.5	.5301
				13.0	1.065	13.0	.5626
				13.5	3.321	13.5	.6130
						14.0	1.058
						14.5	3.564

Table 5 AC Volt-Ampere Characteristics Test Values

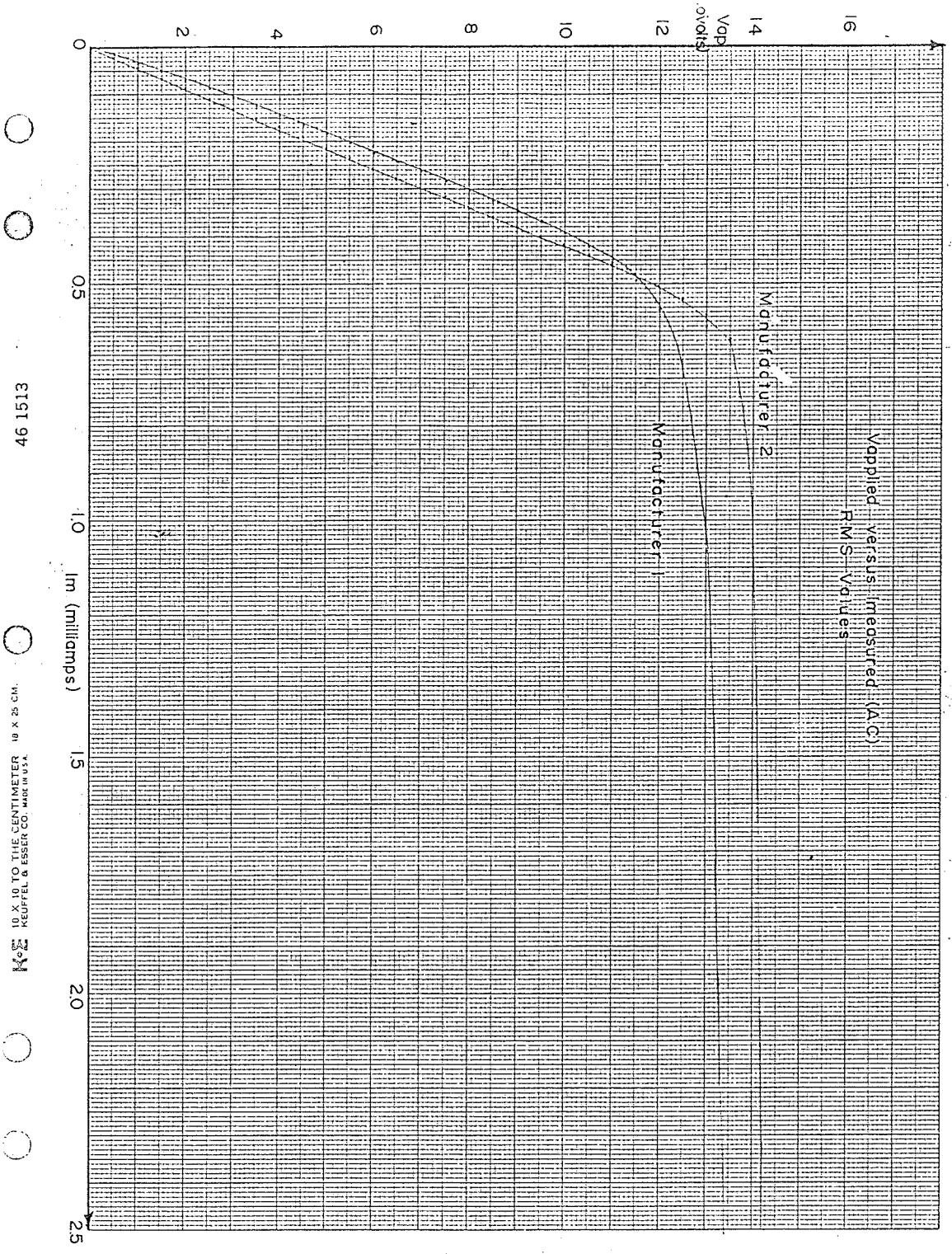

Figure 7 AC Volt-Ampere Characteristics Plots

2.2.3 Impulse Voltage Characteristics

Figure 8 illustrates the test setup for determining the volt-ampere characteristics under a impulse voltage waveform. The results are listed in Table 6 and a small portion of the results in Figures 9-14 in the form of current and voltage oscillograms. The initial unloaded waveshape, that is without the arrestor in the circuit, was 1.25 x 47 microseconds; which is per Institute of Electrical and Electronic Engineers, IEEE, standards and is a wave with a virtual front time of 1.25 microseconds and a half time of 47 microseconds. This voltage is considered to be applied to the arrestor since it is difficult to determine the voltage applied across the surge protective device since the arrestor effectively clips the impulse voltage waveform.

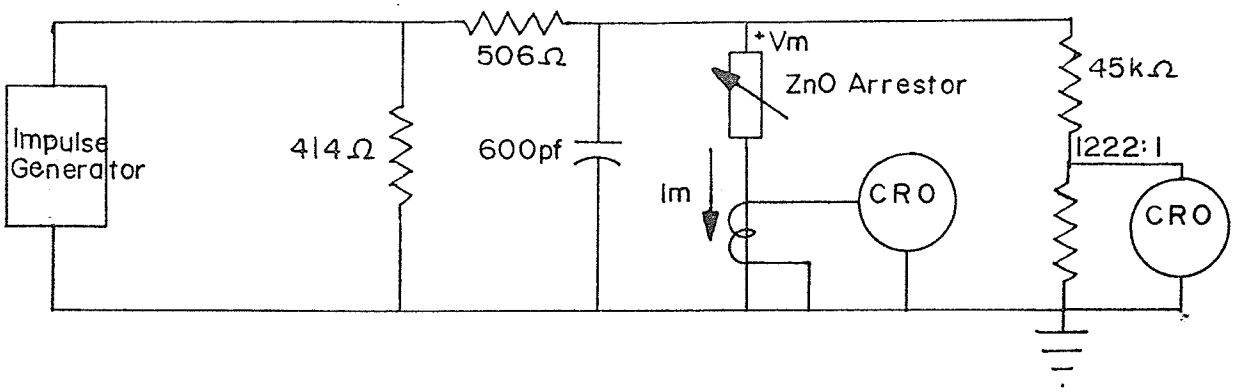

Figure 8 Impulse Voltage Characteristics Test Arrangement

Manufacturer 1						Manufacturer 2		
1 block			2 blocks			3 blocks		
Vc	Vm	Im	Vc	Vm	Im	Vc	Vm	Im
4.0	6.6	6.0	8.0	13.4	3.8	18.5	18.5	1.2
6.0	8.6	6.4	10.0	15.2	7.4	21.0	21.0	5.0
8.0	9.3	18.5	15.0	15.2	11.6	23.5	22.0	8.3
10.0	9.3	22.0	18.5	15.2	46.0	26.0	23.2	13.6
15.0	9.3	54.0	21.0	15.4	78.0	28.5	23.8	20.0
18.5	10.5	83.0	23.5	15.4	90.0	31.0	24.1	22.5
21.0	10.5	96.0				35.0	27.0	29.0
						40.0	28.1	43.0
						50.0	28.4	70.0

Manufacturer 2		
3 blocks		
Vc	Vm	Im
20.0	20.0	1.0
22.5	22.5	2.4
25.0	24.4	6.0
27.5	25.1	13.0
30.0	25.7	18.5
32.5	26.3	20.0
35.0	26.8	31.0
40.0	26.9	33.0
50.0	26.9	50.0

where Vc= impulse generator capacitor voltage in kilovolts
Vm= voltage measured across the arrestor in kilovolts
Im= current measured in the arrestor in amps

Table 6 Impulse Voltage Characteristics Test Values

6110
volts/division

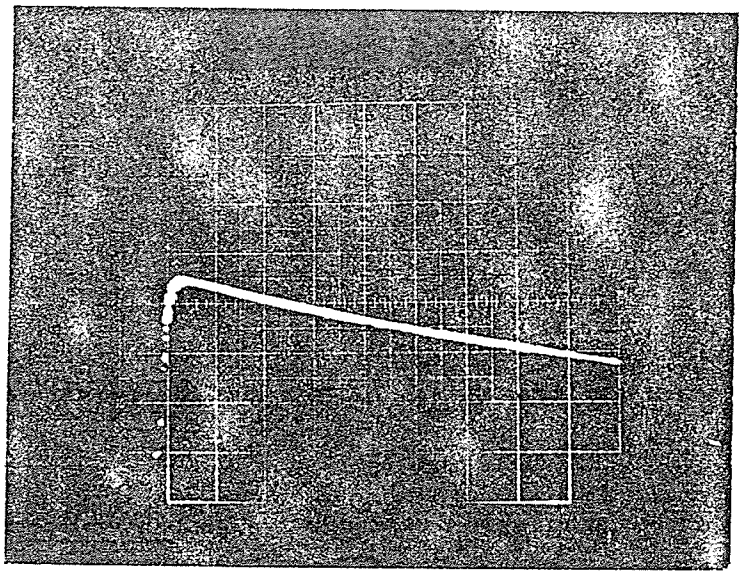

5 microseconds/division

Figure 9 Voltage Oscillogram 20 kV Charging Voltage

amps/division

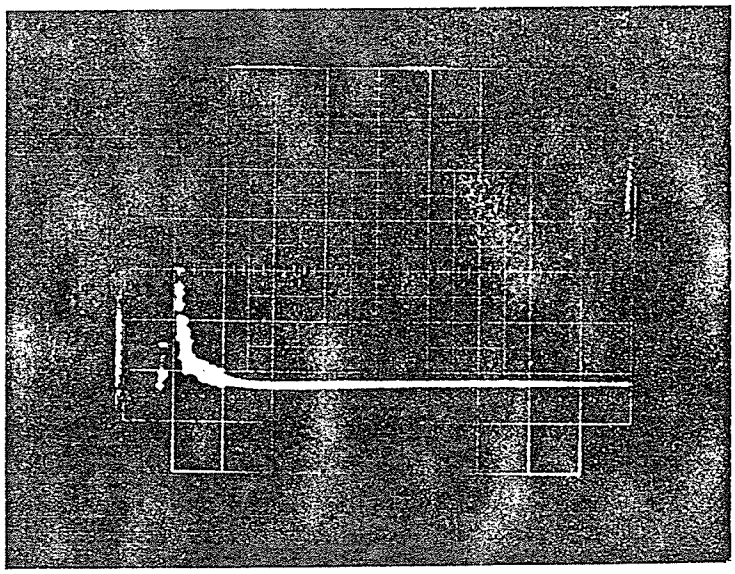

5 microseconds/division

Figure 10 Current Oscillogram 20 kV Charging Voltage

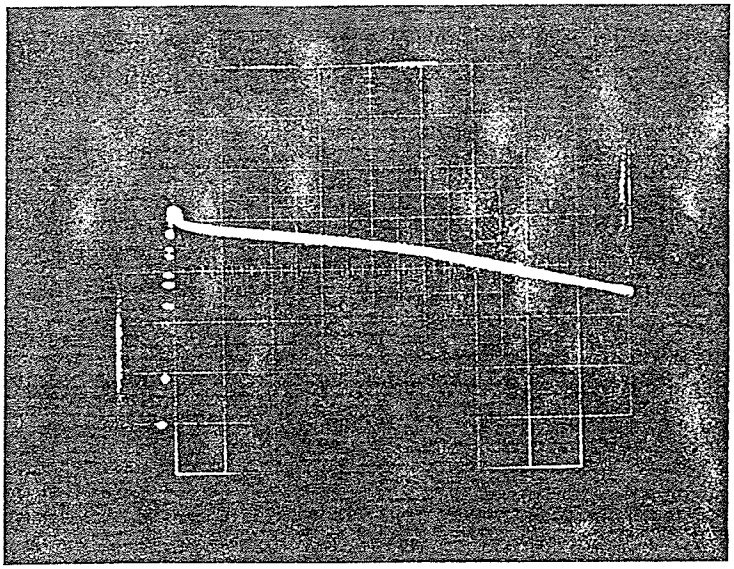

6110
volts/division

5 microseconds/division

Figure 11 Voltage Oscillogram 30 kV Charging Voltage

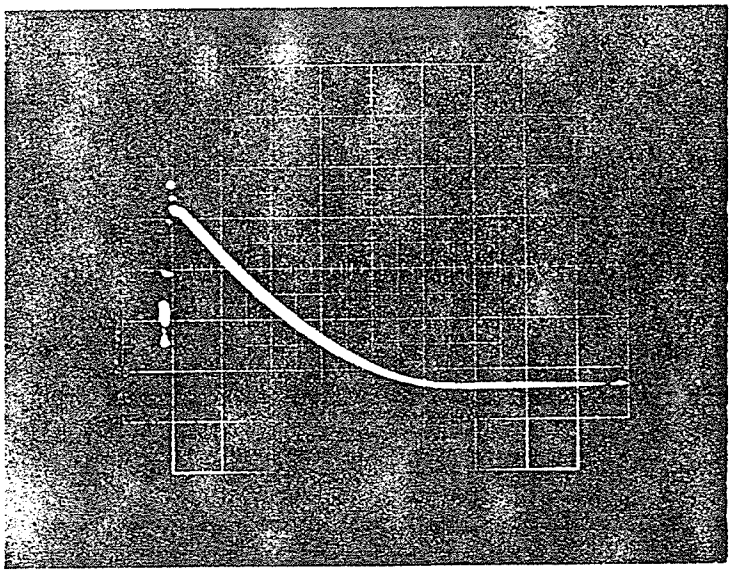

5
amps/division

5 microseconds/division

Figure 12 Current Oscillogram 30 kV Charging Voltage

6110
volts/division

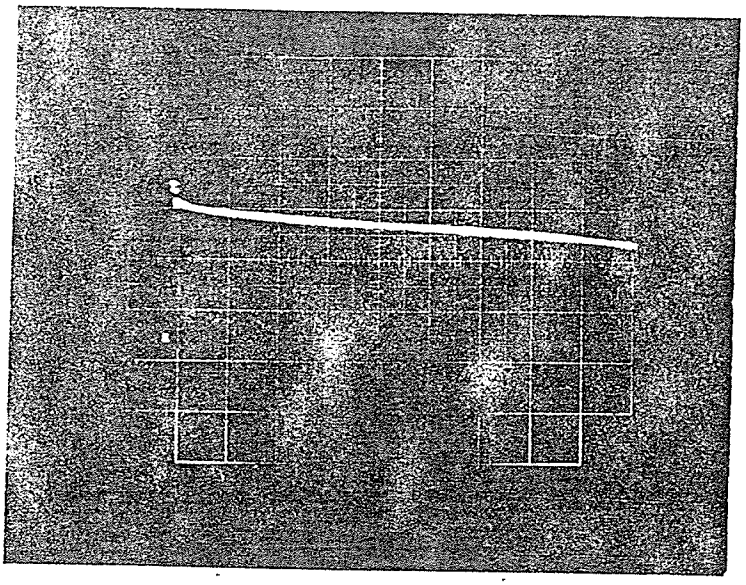

5 microseconds/division

Figure 13 Voltage Oscillogram 50 kV Charging Voltage

10
amps/division

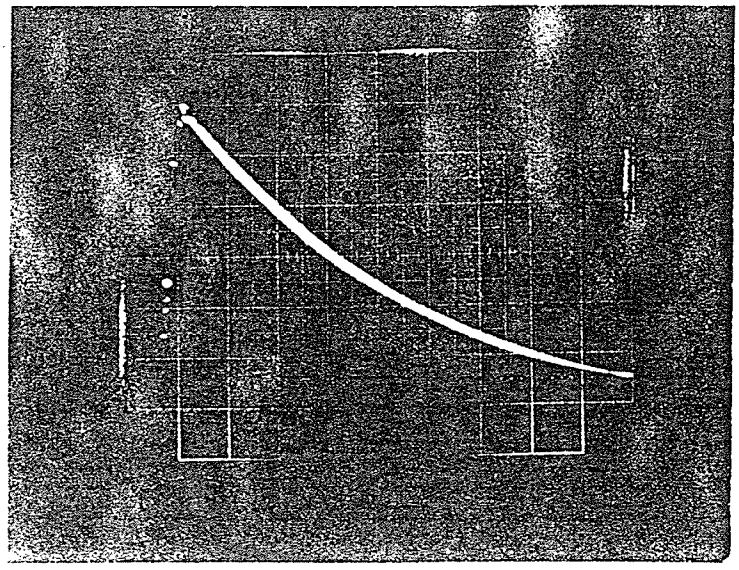

5 microseconds/division

Figure 14 Current Oscillogram 50 kV Charging Voltage

The oscillograms are extremely valuable as they provide a detailed look at the effect of a surge protection device on the actual voltage waveform. Figures 9-14 show the voltage waveform and alternately the resulting current waveform for increasing charging voltages on the impulse generator. It is interesting to observe how the voltage is limited by the arrestor; initially there occurs a small peak which occurs during the first few microseconds; the voltage then levels off and finally decreases to zero. It would appear that the small peak is due to the large initial rate of rise of the current surge which produces a larger discharge voltage. The point at which the voltage begins to decay is a function of the charging voltage. As the charging voltage is increased, the portion of the impulse voltage waveform which is greater than the maximum continuous operating voltage also increases. Therefore the time at which the waveform begins to decay also increases resulting in larger protective device energy absorption. It should be noted that the maximum value of the peak voltage increases only a few kilovolts while the charging voltage doubles. Naturally as the time to decay increases so does the duration of the device current and its magnitude. A quick check of the voltage and current waveforms for a given charging voltage shows that the voltage trace follows the standard impulse waveshape once the current has decreased to zero. The energy absorbed by the surge protection device is simply as shown in Equation 3.

$$\text{Energy} = \int vi\,dt \qquad 3)$$

The impulse voltage tests were performed on one, two, and three block sections and the linearity of zinc oxide blocks are illustrated. Therefore, the impedance would appear to be entirely resistive since the current flowing through three blocks is one third the value of the current flowing through one block at a given voltage.

A curve fitting program was again utilized to determine the value of b in Equation 2. For manufacturer 1, b was found to be approximately 10 while for manufacturer 2 this value was approximately 12. In addition to the previously mentioned reasons, it was extremely difficult to determine the actual voltage applied to the arrestor and therefore, the voltage levels used in obtaining the value of b may have resulted in some error.

2.2.4 Impulse Current Characteristics

Figure 15 illustrates the test setup for the impulse current testing. The 31 microhenry inductor was included in the circuit to produce an 8x20 microsecond impulse current waveform; which has a virtual time to crest of 8 microseconds and half time of 20 microseconds. Tests were also performed without the inductor to illustrate the effects of a fast front waveform on the discharge voltage level of the blocks. The results are tabulated in Table 7; a portion the oscillograms are shown in Figures 16 to 21.

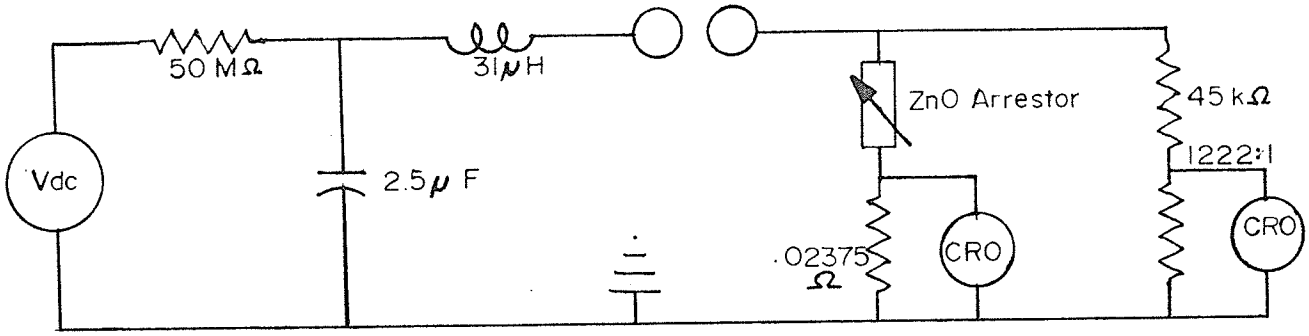

Figure 15 Impulse Current Characteristics Test Arrangement

	Manufacturer 1			Manufacturer 2
1 block	2 blocks		3 blocks	3 blocks
Is * Vm	Is * Vm		Is * Vm	Is * Vm
**********	**********		**********	**********
1.5 * 9.5	1.5 * 18.3		1.5 * 26.3	1.5 * 13.0
5.0 * 10.9				5.0 * 13.9

where Is= value of the impulse current surge in kiloamps

Vm= discharge voltage measured in kilovolts

Table 7 Impulse Current Characteristics Test Values for Slow Front Current Wave

2105
amps/division

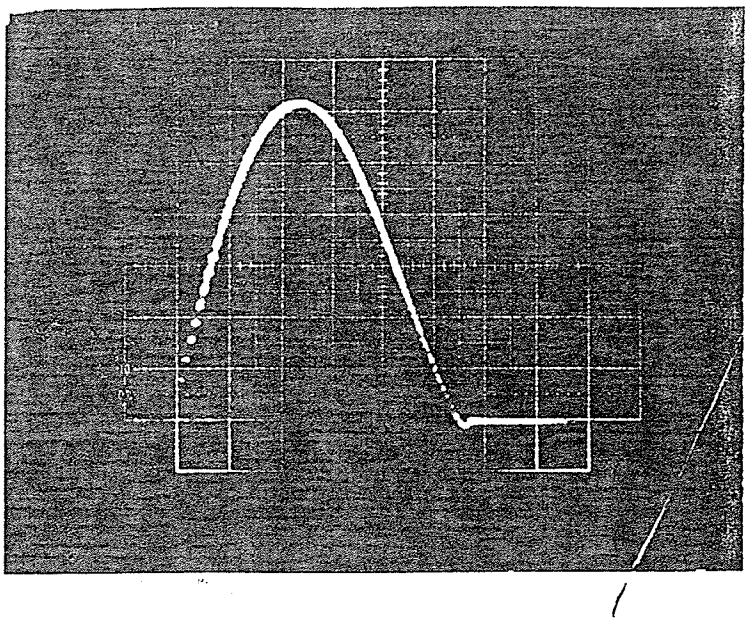

1 microseconds/division

Figure 16 Current Oscillogram Without the Waveshaping Inductance
21.5 kV Triggering Voltage for Fast Front Current Wave

2444
volts/division

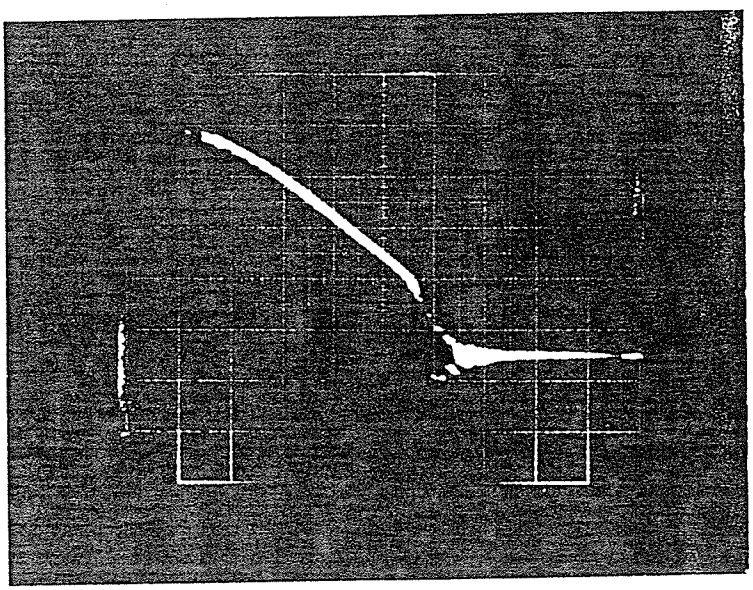

5 microseconds/division

Figure 17 Voltage Oscillogram Without the Waveshaping Inductance
21.5 kV Triggering Voltage for Fast Front Current Wave

421
amps/division

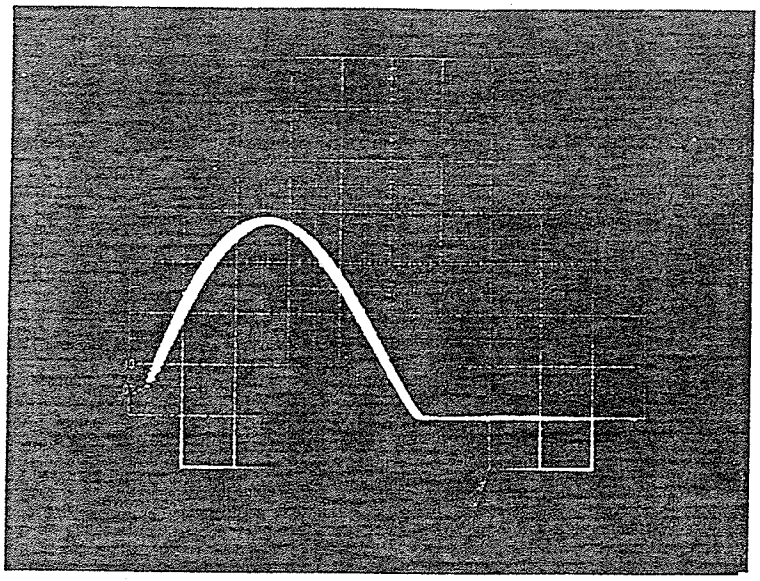

5 microseconds/division

Figure 18 Current Oscillogram 15 kV Triggering Voltage for Slow Front Current Wave

2444
volts/division

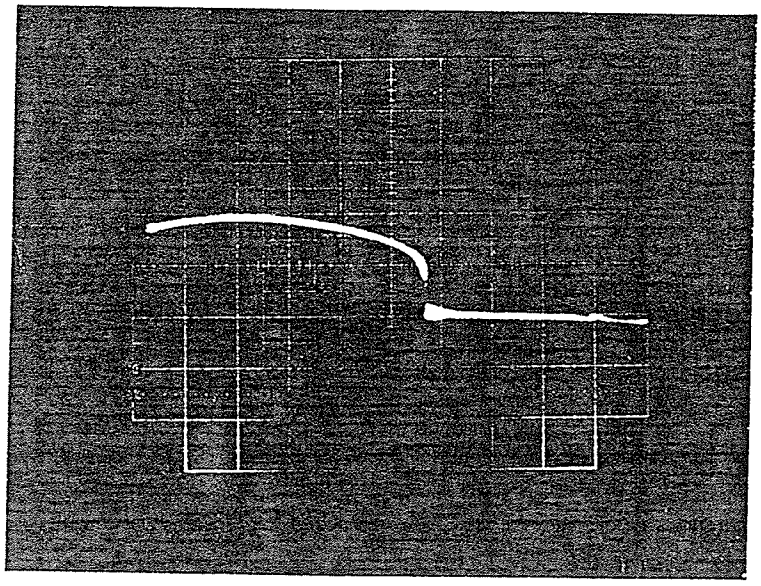

5 microseconds/division

Figure 19 Voltage Oscillogram 15 kV Triggering Voltage for Slow Front Current Wave

942
amps/division

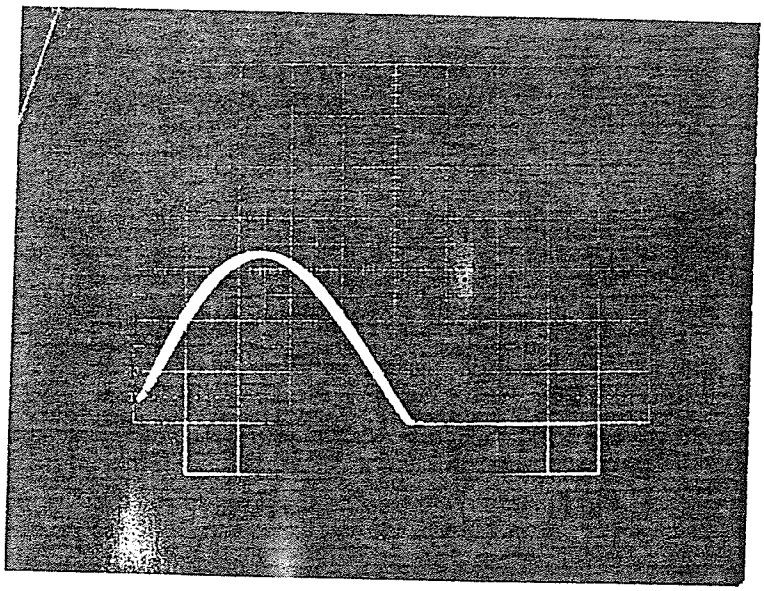

5 microseconds/division

Figure 20 Current Oscillogram 20 kV Triggering Voltage for Slow Front Current Wave

2444
volts/division

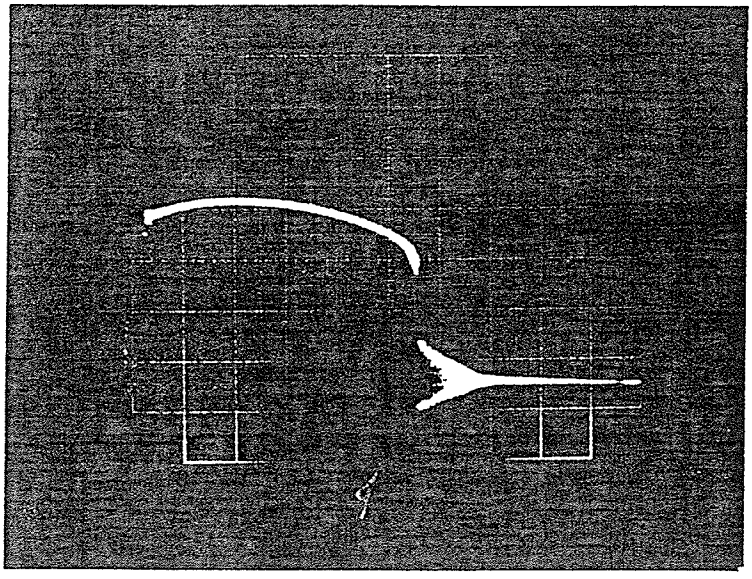

5 microseconds/division

Figure 21 Voltage Oscillogram 20 kV Triggering Voltage for Slow Front Current Wave

It is apparent from Table 7 that again the impedances of the individual blocks add linearly. The value of b in Equation 2 was found to be approximately 10 for manufacturer 1 while for manufacturer 2, it was approximately 17. From all the volt-ampere characteristics it is obvious the Equation 2 is valid for only portions of the curve and to model a ZnO arrestor at least three separate values of a and b must be used. One set of values for the leakage current range is needed while another is required for the highly non-linear range and finally another set of values is required for the upturn portion of the curve. From the relevant literature, it is suggested that all these values can be obtained from impulse current tests since a current wave is not clipped.[8] However, with the test setup it was impossible to perform all these tests due to the energy limitations of the impulse current generator.

The oscillograms show the current surge and then the corresponding discharge voltage waveform. This is a very important insulation coordination criteria because it is the discharge voltage levels which determine the protective margin provided by the surge protection device. It is interesting to note the dependence of the voltage waveform on the impulse current waveshape. For faster front waveforms, Figures 16 and 17, the discharge voltage rises very quickly to a peak, within half a microsecond, and then decays linearly and finally drops with substantial ringing. The ringing is due to the presence of

inductance and capacitance in the test and measuring circuit. However, it should be noted that in most cases the voltage does not decrease to zero within the time frame of the oscillogram. Depending upon the magnitude of the current surge, there is some residual voltage across the ZnO block. The magnitude of this residual voltage is linked to the amount of charge which flows through the arrestor. For a large current surge the proportion of charge drained is much greater than for a lower magnitude of surge. In other words the greater the magnitude of the current surge the lower the final value of the discharge voltage in the oscillogram.

With the 8x20 microsecond impulse current waveform, Figures 18 and 20, the rate of rise of the discharge voltage waveform is initially large; it then decreases as the peak voltage value is reached. Next the rate becomes a small negative value and this continues until conduction ceases in the arrestor and then it finally becomes a very large negative value until the final voltage level is reached where it returns to zero. The reason for the difference between this waveform and that due to a faster current surge is due to the presence of the 31 microhenry inductor in the test circuit. This inductor limits the rate of change of current and consequently the appearance of the voltage waveform.

2.3 Thermal Tests

Both General Electric and Ohio Brass, two under-oil arrestor manufacturers, have performed accelerated ageing tests on their respective under oil arrestor assemblies. The life of the assembly has been found to exceed 100 years.[25] As well the Arrehnius plots of the accelerated ageing tests resemble those of the arrestors in air alone. An example of an Arrehnius plot is shown in Figure 22. The basis for the Arrehnius plot is the relation that the logarithm of insulation life is a function of the reciprocal of temperature. A more detailed description of Arrehnius plots can be found in Appendix 3.

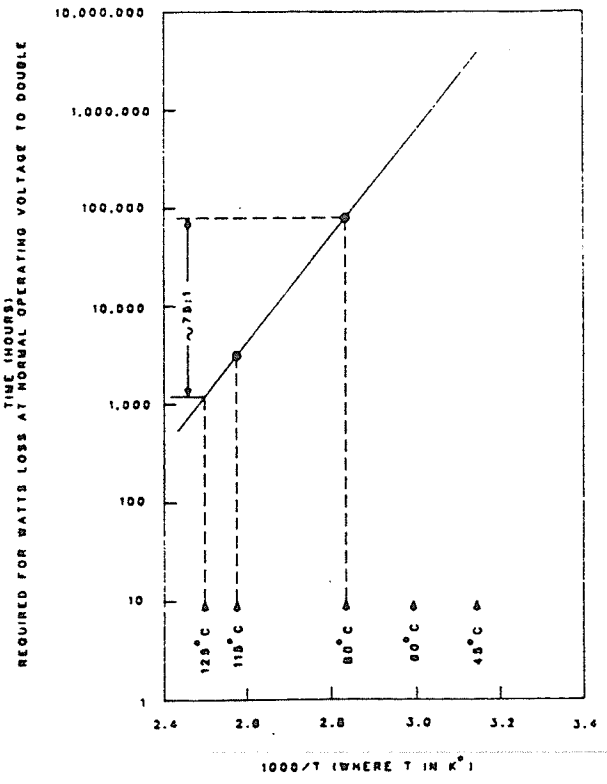

Figure 22 Arrehnius Plot

In addition to the thermal life information obtained from several United States manufacturers, it was decided to perform tests on typical zinc oxide blocks to determine the effect of oil immersion on the blocks. The tests were begun in April 1985 and are still continuing. The test procedure consists of immersing a zinc oxide block in oil and subjecting it to a thermal cycle similar to that experienced daily by a typical distribution transformer under load. That is two peaks of three hours duration at 105 degrees Celsius. In order to determine the peak temperature, some knowledge of the operating temperature of a distribution transformer was required. From Canadian Standards Association, CSA, specifications, the average winding temperature rise for a transformer operated at 100% rating must not exceed 65 degrees celsius. With a hot-spot temperature rise of 10 degrees celsius above average winding rise and an ambient temperature of 30 degrees celsius the value of 105 degrees celsius is obtained. The reason for cycling the temperature was to cause mechanical stresses in the block due to thermal expansion and contraction.

Initially the tests were to be performed on new and aged oil; however, after a little thought it was decided that the tests would only be performed on ZnO blocks immersed in aged oil. Since aged oil has already deteriorated, if the ZnO blocks showed no adverse affects after a lengthy immersion, they should certainly not demonstrate any effects with new oil. Manitoba Hydro generously donated five gallons of oil from a distribution

transformer in service since 1963. The oil was tested at Manitoba Hydro for dissolved water, dielectric strength, neutralization number and interfacial tension and the results are shown in Table 8. It can easily be observed that properties of the aged oil are substantially worse than the new oil and that the aged oil has been degraded. Also when compared to the acceptable standards it is apparent that the aged oil fails for both neutralization number and interfacial tension. The neutralization number is the amount of a base, in this case Potassium Hydroxide, which must be added to a gram of oil to neutralize the acids which have been produced due to the oil ageing. On the other hand interfacial tension is a measure of the amount of weight the surface of the oil can support prior to the weight sinking and the higher the number the better.

	New Oil	Aged Oil	Acceptable Standards[32]
Dissolved Water (parts per million)	12	5.2	
Dielectric Strength (kilovolts) (D1816)	35	50	30
Neutralization Number (milligrams KOH/gram of oil)	0	.04	.03
Interfacial Tension (Dynes/ centimeter)	43	29.2	35

Table 8 Oil Comparison

The blocks were allowed to cycle through the heating and cooling cycle initially for a two week period. Various papers reported that the reaction between the oil and the blocks would occur very shortly after the blocks were immersed in the oil.[25] At the end of the two weeks the volt-ampere characteristics were compared with the original values. The tests were performed at ambient temperature under both AC and DC voltages. No deviation from the original values were observed. The testing commenced in April 1985 and periodic testing is now being carried out monthly. The testing is still continuing today. The most recent results have shown no indication of Zinc Oxide deterioration.

2.3.1 Calculation Of Equivalent Life

The method used to determine the equivalent ageing of the under oil arrestor is given in the proposed ANSI specification C62.11, " Standard for Metal Oxide Surge Arrestors for Alternating Current Power Circuits".[4] Equation 4, the acceleration factor for arrestor life testing was obtained from Appendix 4 of the ANSI specification which is The Basis for Accelerated Ageing Procedure.

$$AF_T = 2.5^{\,T/10} \qquad 4)$$

Where AF_T = acceleration factor

T = Test Temperature - operating temperature (in ^{o}C)

From the tests performed, AF_T has been found to be 24.705, and the equivalent test time to date is approximately 5.23 years at 50 degree Celsius top oil rise. The 50 degree Celsius top oil rise was taken from ANSI specification C57.91, "Guide for Loading Mineral Oil-Immersed Overhead-Type Distribution Transformers with 55 degree Celsius or 65 degree Celsius Average Winding Rise". The value of 24.705 is calculated by subtracting 80 from 105 degrees Celsius and inserting this value in Equation 4. While the value of 5.23 is calculated by multiplying the acceleration factor, 24.705, by 4636 minutes of actual test time at 105 degrees Celsius.

3. Zinc Oxide Under Oil Arrestors

3.1 Installation

It is possible to order ZnO under-oil arrestors with any desired terminal mounting arrangement. As mentioned earlier the arrestor is housed in a phenolic tubing approximately a quarter of an inch thick. This provides sufficient dielectric strength to allow the arrestor assembly to be placed anywhere within the tank provided that the whole assembly is beneath the oil surface. Another important criteria is to minimize lead lengths and to maintain adequate clearances between the arrestor terminals and grounded objects. A possible location is between the coils of a core-type transformer or above the core and coil clamping structure. The location of the arrestor is related to tank size and oil height because a transformer manufacturer for economical reasons, is reluctant to add extra material resulting in a larger tank and increased oil capacity. Figure 23 shows the location of the under-oil arrestor in a single phase core-type core and assembly. The completed assembly is nearly of the same size as a single phase unit without the arrestor. Also the lead length is negligible meaning that the discharge voltages produced by the arrestor provide the largest margin.

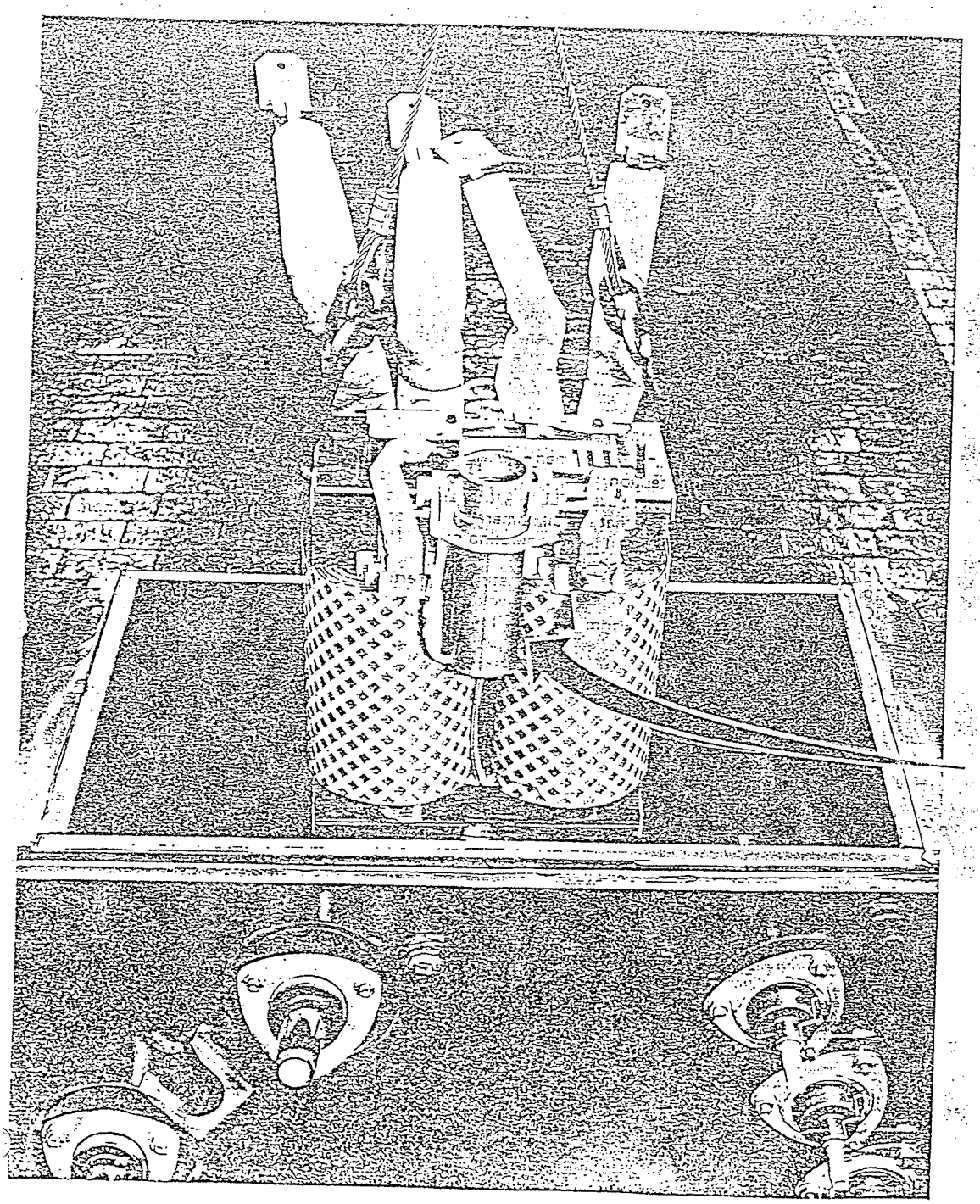

Figure 23 Under Oil Arrestor Locating

3.2 Arrestor Monitoring

In order to determine the operational status of a lightning arrestor there must be a method of checking the arrestor in service. Through discussions with various utilities regarding arrestor monitoring it is possible to draw some conclusions. Most utilities install a ground lead disconnect device on their arrestors. Should a surge of sufficient magnitude occur, the explosive cartridge in the device automatically disconnects the ground from the arrestor. If a maintenance crew member notices that the ground lead is no longer connected to the arrestor, the arrestor is eventually replaced. Since the cost of continuous arrestor monitoring at the distribution level would be a substantial percentage of the purchase price of the transformer, the impetus for monitoring arrestors is not evident.

Despite utility reluctance for distribution arrestor monitoring two possible method are now presented. The first method is simply an extension of the ground lead disconnect for overhead distribution transformers while the second is more innovative but is rather costly and therefore unlikely to get utility support.

3.2.1 Ground Lead Disconnect

Instead of grounding the under-oil arrestor directly to the tank, a ground lead must be brought out through an insulated bushing. Connected to the bushing is a ground disconnect device which separates the ground lead from the bushing once a surge, whose energy level exceeds the allowed design value, passes through the arrestor. The procedure for detection and replacement of the arrestor is the same as the current utility procedure. A disadvantage of this system is the introduction of additional arrestor lead length.

3.2.2 Modern Method

Figure 24, a block circuit diagram, illustrates a sophisticated method for monitoring arrestors, which indicates the operation and failure of the arrestor. The current measuring device in the ground lead circuit is a Hall Effect device which produces a voltage proportional to the current flowing in the ground lead. Under normal conditions this voltage, which is very small is measured by the level detection device and a five volt signal is sent to a JK flip-flop which holds the value for sampling by the computer. Once the arrestor fails, the flip-flop is reset to zero and at the next time step the value is sent to the computer. Once a surge current greater than 1 kiloamp flows through the arrestor another voltage level detector goes high and the output is sent

to another flip-flop which holds the values for computer sampling. This JK flip-flop is also reset when the surge has passed. In addition to the aforementioned circuit devices a power supply is required. It is quite easy to obtain the necessary voltage requirements by simply adding the necessary turns through the core and utilizing a full-wave bridge with a filter.

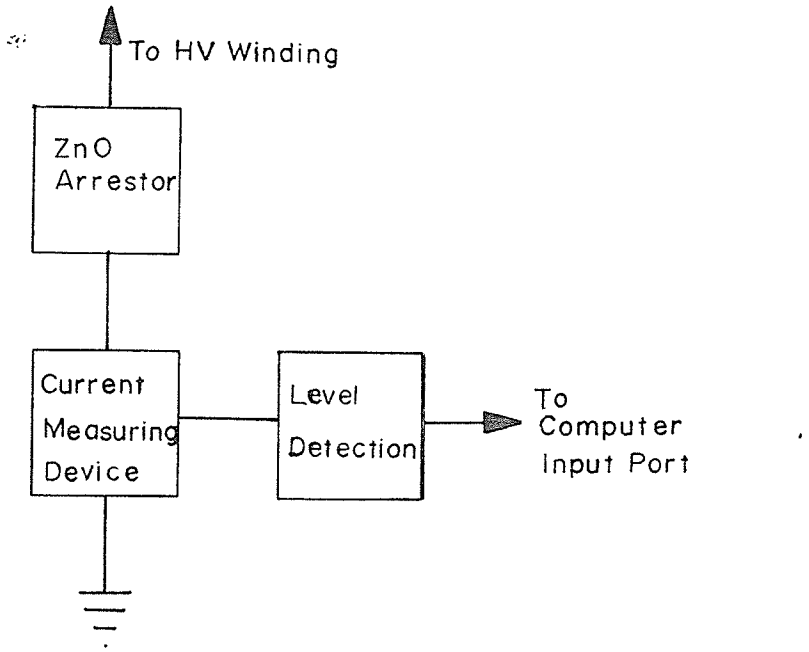

Figure 24 Arrestor Failure Detection Circuit

3.3 Recurrent Surge Generator Tests

To examine the effects of an under-oil arrestor on the voltage distribution along the winding of an actual transformer, low voltage recurrent surge testing was performed on an distribution class transformer's untanked core and coil assembly. The transformer tested was a core-type unit which has a wound core and two coils; one on each leg of the core. This is a typical design of a distribution class transformer at Carte Electric Ltd.. The actual transformer specifications are single phase, 75 kVA, 7200-120/240 volts, 65 degree celsius average winding rise, oil filled, pole-type distribution class transformer with off load taps of 4-2.5%, two full capacity above normal and two reduced capacity below normal. A metal oxide varistor, a low voltage surge protection device, simulated the ZnO arrestor and surges were applied by using a low voltage recurrent surge generator, RSG. These RSG tests were performed with and without the surge protection device connected across the high voltage winding.

The maximum continuous operating voltage, MCOV, of the metal oxide varistor was chosen such that the 1 kilovolt output of the RSG would resemble a 95 kilovolt impulse waveform. In order to accurately model the performance of an actual arrestor-transformer system the low voltage tests must be scaled to resemble the actual system. By using the ratio of the surge test

values it was determined that the maximum continuous operating voltage for the metal oxide varistor should be approximately 140 volts. For this test a 20 percent safety margin, typical of the value employed by utilities, for any temporary power frequency overvoltages was provided. It is widely accepted in industry that except for some possible non-linearity of core saturation the measured values can be scaled to actual voltages by multiplying them by the ratio of actual to test voltage.[28]

Figure 25 illustrates the test setup. Both layer to ground and layer to layer voltages were determined for a standard impulse with and without protection. The same tests were also repeated with a chopped impulse waveform. A standard impulse impulse in this instance had a virtual front time of 1 microsecond and a time to half value of 45 microseconds, while the chopped impulse had a virtual front time of 1 microsecond and a time to chop of 3 microseconds. Due to difficulty in probing beneath the core and coil assembly only the top of each layer of a winding was accessed; therefore, every second layer was measured. However, for layer to layer voltage stresses the measurements obtained are an indication of the worst case to be expected.

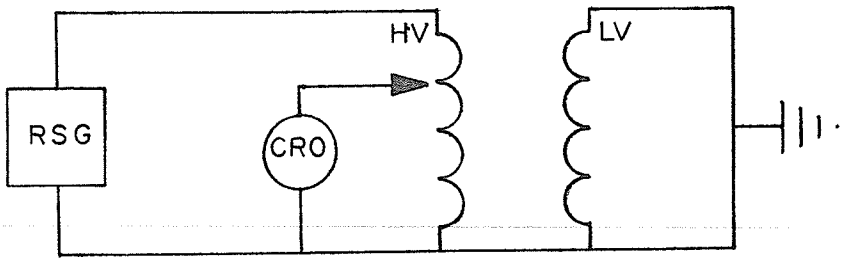

Figure 25 Recurrent Surge Generator Test Arrangement

3.3.1 Full Wave Tests Layer-To-Ground

Table 9 shows the test results obtained with a full wave impulse applied to the line terminal in Figure 24. The voltages in Table 9 are measured with respect to ground. Comparing the results obtained with and without the arrestor, it becomes obvious that the arrestor severely limits the maximum voltage applied to the transformer coils to 34 percent of 95 kilovolts, that is 32.3 kilovolts. This reduction of 66 percent provides a transformer design engineer with large safety margins which can be reduced as will be seen later in this thesis. As other values in Table 9 are compared, it is observed that there are again substantial voltage reductions throughout the winding; however, as the distance from the line terminal increases, the reduction in voltage to ground decreases. A quick check of the values obtained in Table 9 can be performed by multiplying the full wave, no arrestor percentages, column 2, by .34. As expected this gives approximately, the full wave arrestor percentages, column 3.

Probe Location	Without Arrestor Voltage(% of Line End)	With Arrestor Voltage(% of Line End)
Line End	100	34
18l	94	32
16l	74	24
14l	53	20
12l	47	17
12r	44	11
14r	32	9
16r	18	7
18r	4	2

where 18l means layer 8 left leg and 16r means layer 6 right leg et cetera

Table 9 Full Wave Layer-to-Ground Test Results

3.3.2 Full Wave Test Layer-to-Layer

The voltages measured between consecutive layers of the transformer are presented in Table 10. Without any overvoltage protection the maximum voltage between layers was 30 percent of 95 kilovolts, that is 28.5 kilovolts. This peak occurred between layers four and two of the left leg coil. The corresponding maximum value for the coil with voltage protection occurred in the same location, but the value was only 10% of 95 kilovolts, 9.5 kilovolts. Once again as illustrated in Table 10 the design engineer may safely reduce insulation thicknesses.

Probe Location	Without Arrestor Voltage(% of Line End)	With Arrestor Voltage(% of Line End)
line-18l	8	4
18l-16l	22	8
16l-14l	23	6
14l-12l	30	10
12l-12r	13	9
12r-14r	14	4
14r-16r	15	4
16r-18r	13	5

where 18l means layer 8 left leg and 16r means layer 6 right leg et cetera

Table 10 Full Wave Layer-to-Layer Test Results

The results from Tables 9 and 10 are plotted in Figure 26. The layer-to-ground voltages are shown as circles or triangles while the layer-to-layer voltages are shown as dotted or full lines. Such plots are very useful to transformer design engineers as it enables them to ensure that there is adequate insulation between various components of the winding. It is interesting to note that the voltage distribution within the winding is not linear. Generally, the maximum layer-to-layer voltage does not occur at the line end of a winding but rather somewhere within the winding. This is due to travelling waves reflecting at the grounded end which produces dissimilar oscillations in the different layers of the winding that are quite different between layers.

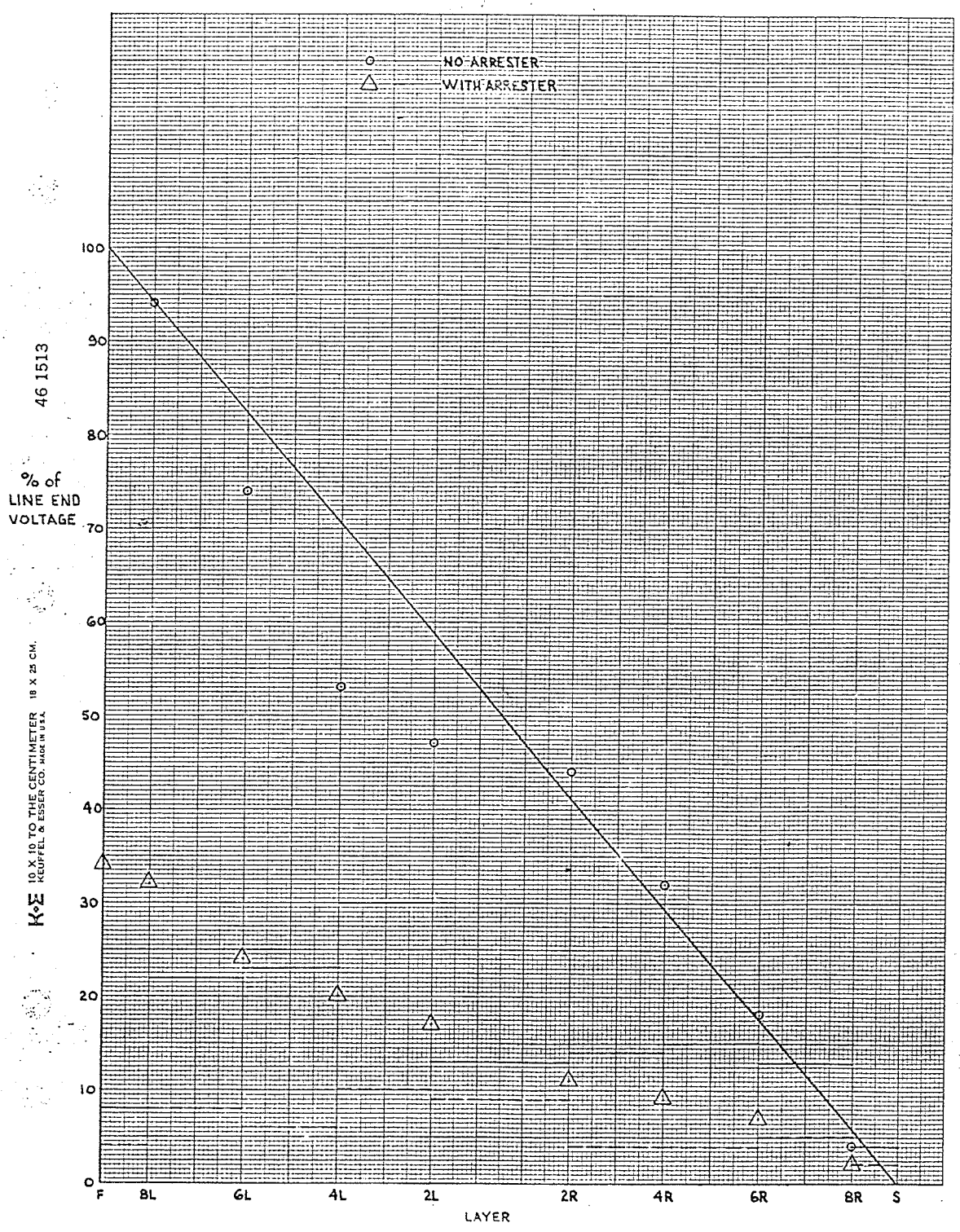

Figure 26 Full Wave Voltage Distribution in a Transformer Winding

Figures 28 to 38 are the oscillograms at various points in the winding and they show, alternately, voltage from layer-to-ground and layer-to-layer voltages. The sharp peaks on the tests performed with the arrestor are due to the initial rapid rate of voltage rise. By careful observation of oscillograms the travelling waves and its effect on the layer to layer voltages can be seen.

20% per
division

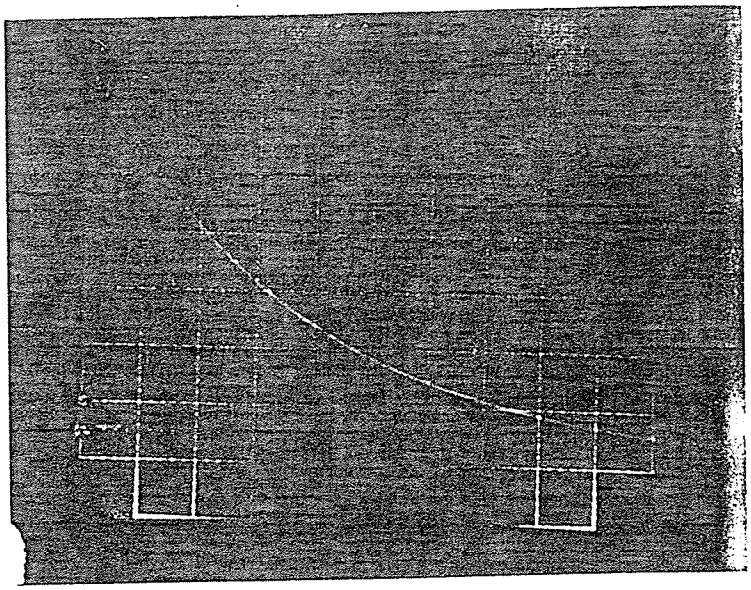

20 microseconds/division

Figure 27 Line-to-Ground Voltage No Arrestor

20% per
division

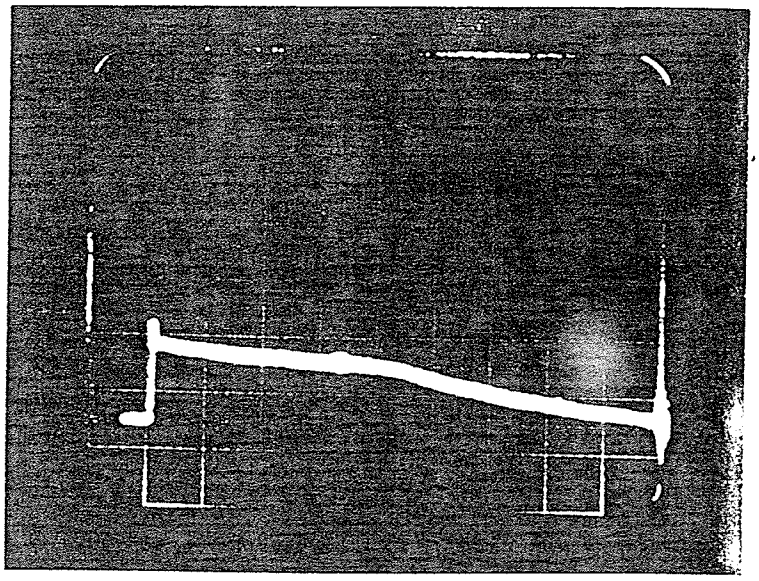

20 microseconds/division

Figure 28 Line-to-Ground Voltage With Arrestor

20% per
division

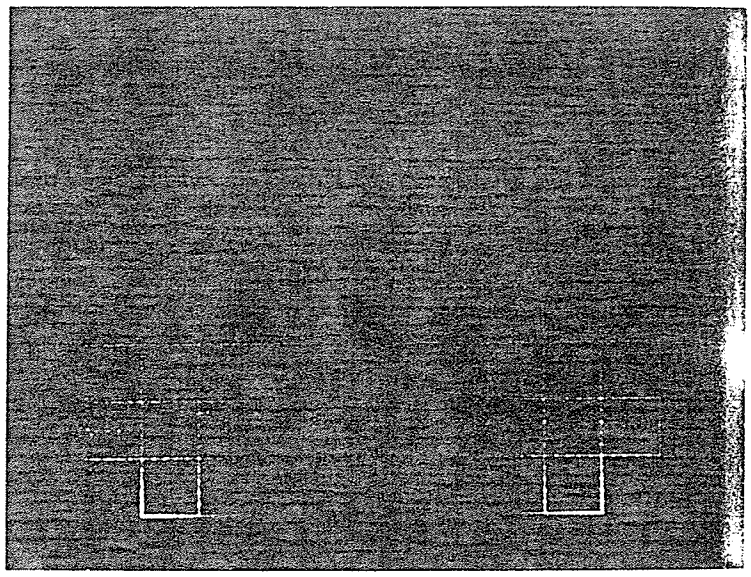

20 microseconds/division

Figure 29 Layer 2, Left Leg-to-Ground Voltage No Arrestor

20% per
division

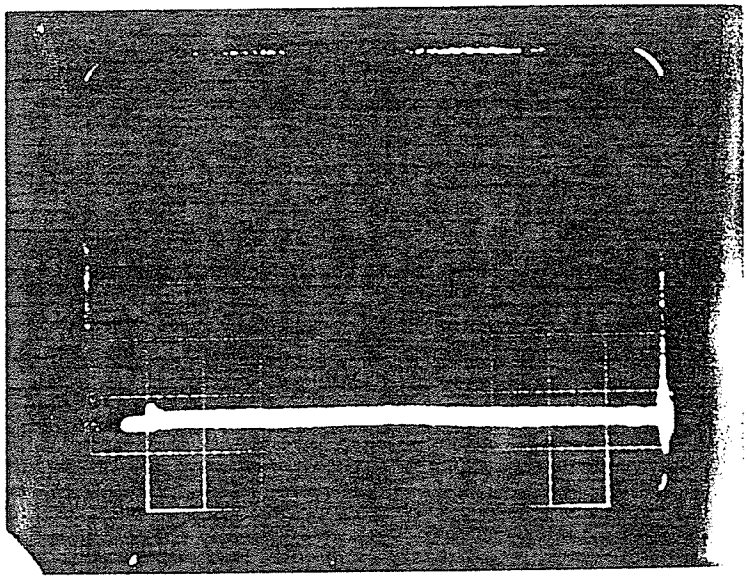

20 microseconds/division

Figure 30 Layer 2, Left Leg-to-Ground Voltage With Arrestor

20% per
division

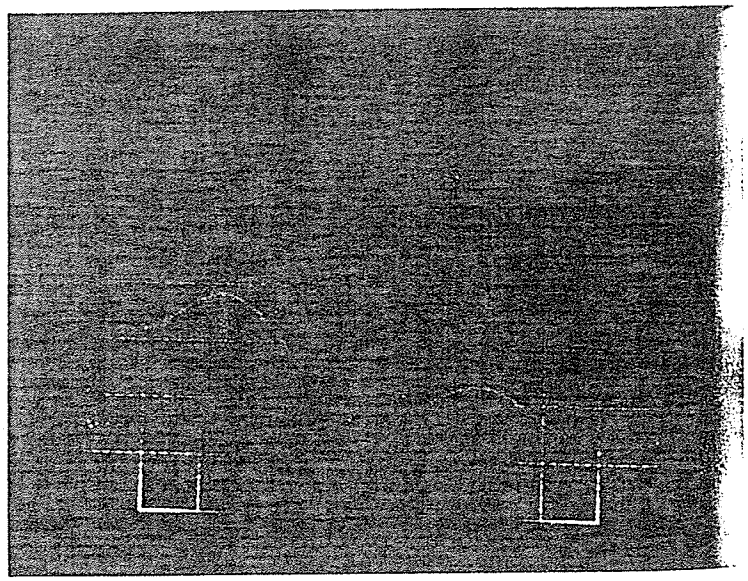

20 microseconds/division

Figure 31 Layer 6, Right Leg-to-Ground Voltage No Arrestor

20% per
division

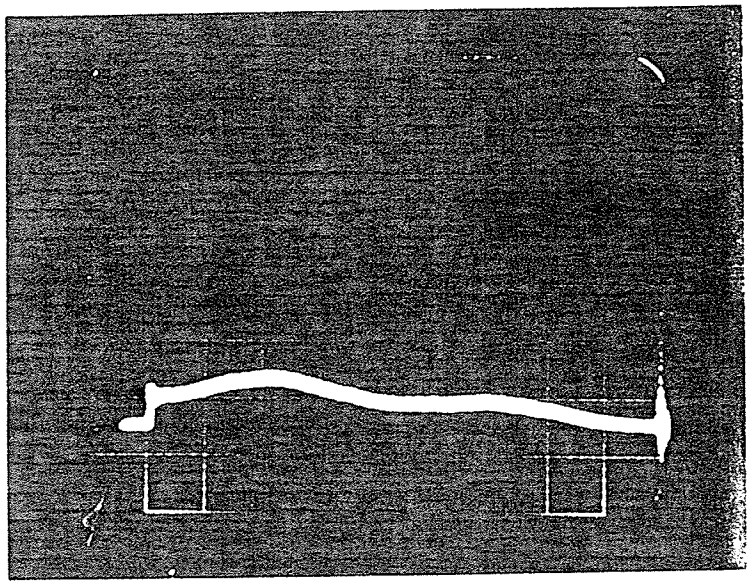

20 microseconds/division

Figure 32 Layer 6, Right Leg-to-Ground Voltage With Arrestor

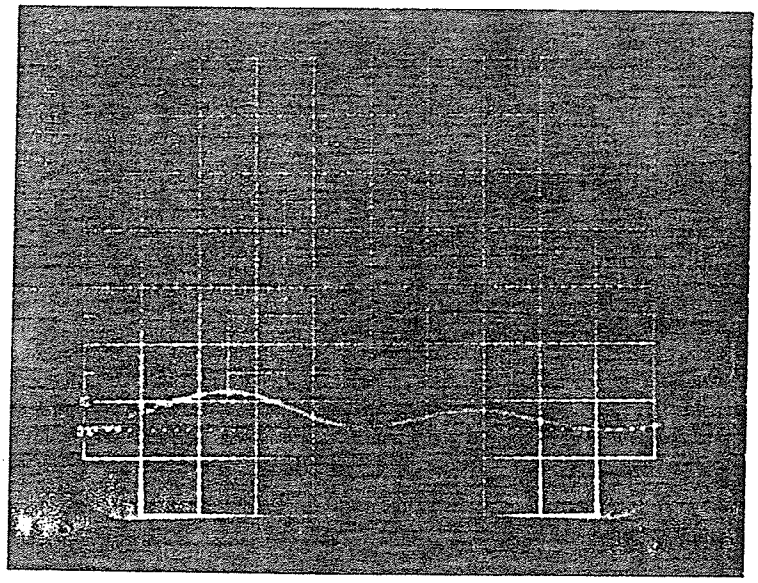

20% per division

20 microseconds/division

Figure 33 Line-to-Layer 8, Left Leg Voltage No Arrestor

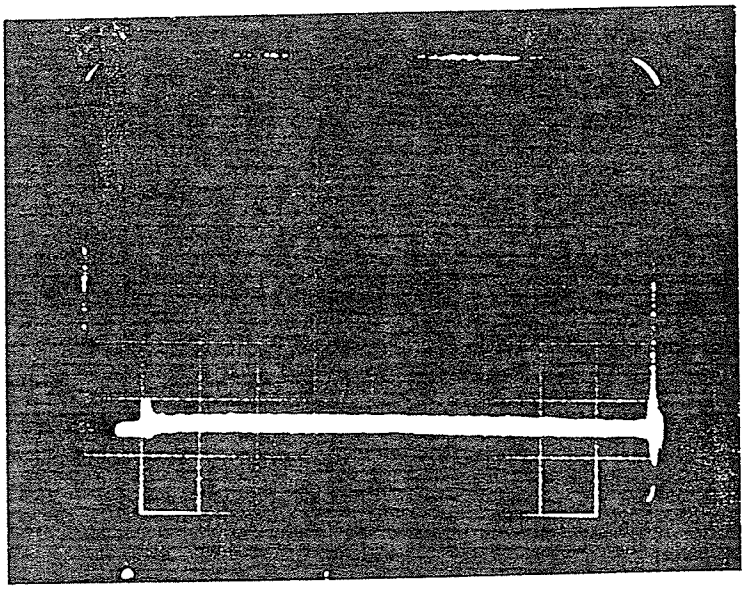

20% per division

20 microseconds/division

Figure 34 Line-to-Layer 8, Right Leg Voltage With Arrestor

20% per division

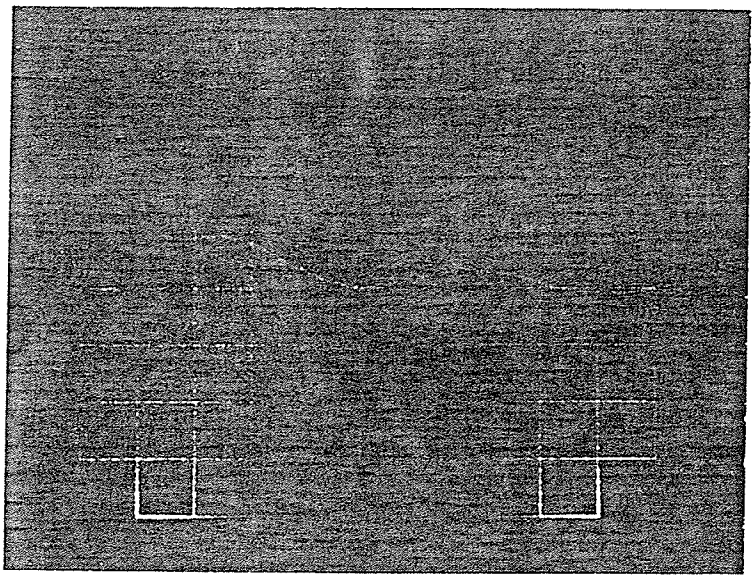

20 microseconds/division

Figure 35 Layer 2, Left Leg-to-Layer 2, Right Leg Voltage No Arrestor

20% per division

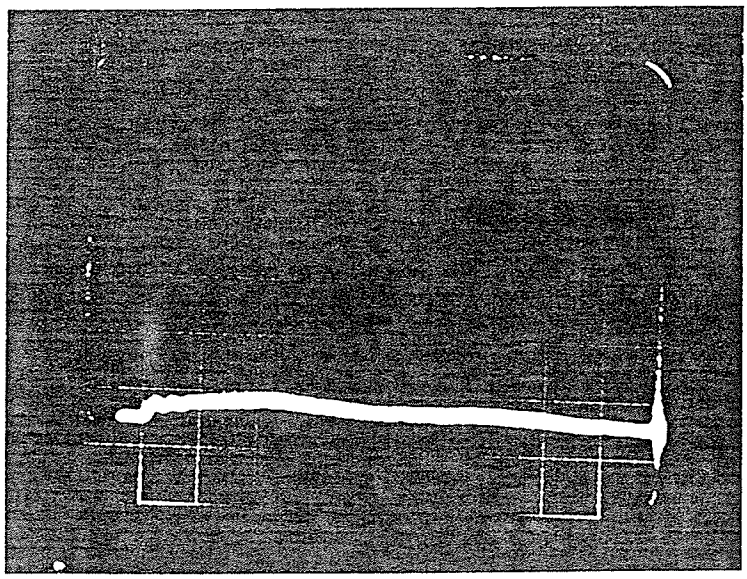

20 microseconds/division

Figure 36 Layer 2, Left Leg-to-Layer 2, Right Leg Voltage With Arrestor

20% per division

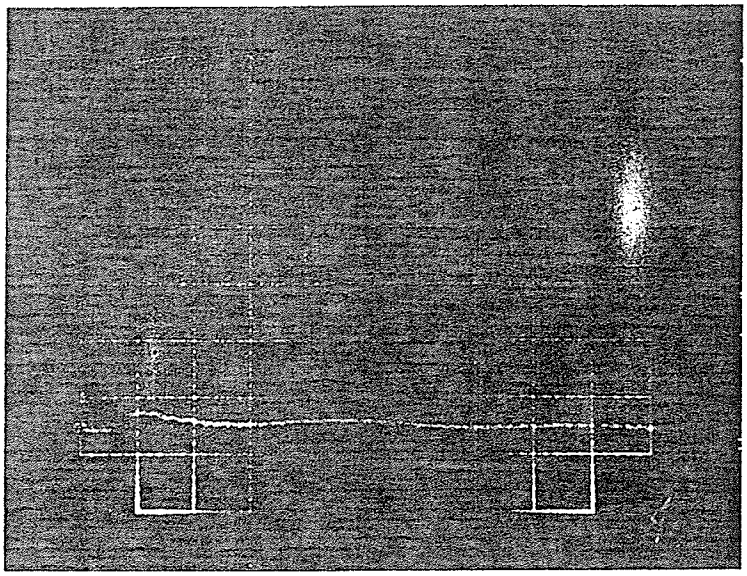

20 microseconds/division

Figure 37 Layer 6, Right Leg-to-Layer 8, Right Leg Voltage No Arrestor

20% per division

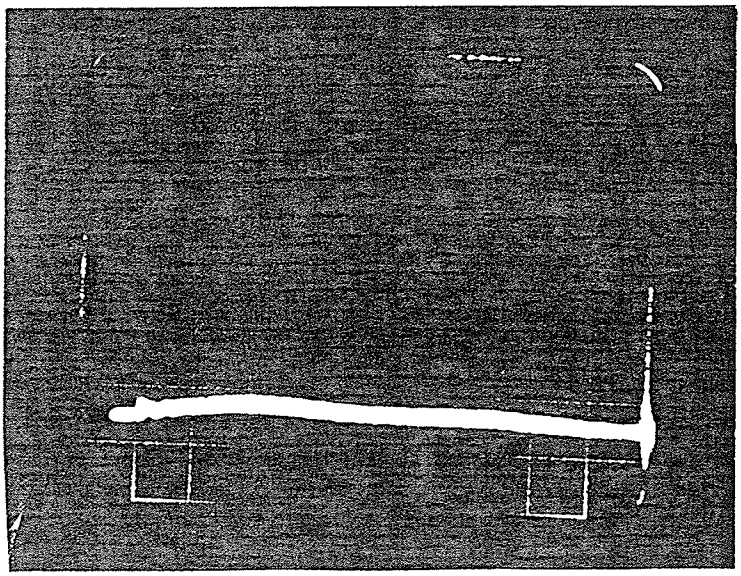

20 microseconds/division

Figure 38 Layer 6, Right Leg-to-Layer 8, Right Leg Voltage With Arrestor

3.3.3 Chopped Wave Tests Layer-To-Ground

Next, testing of the transformer core and coil assembly was conducted with the chopped impulse voltage waveform. Table 11 lists the results of the test and by comparing this results with those in Table 9 it is apparent that the voltage distribution due to a chopped waveform has a higher degree of non-linearity. A Fourier analysis of the full and chopped wave forms would show the presence of higher frequency components in the latter case. Since the initial voltage distribution is determined by capacitances, which are frequency dependent, the voltage distributions of a transformer winding under full wave or chopped impulse are expected to be dissimilar. The maximum value, with the arrestor, seen by the winding is 35 percent of 95 kilovolts, 33.25 kilovolts. This value, within the range of error introduced by determining the magnitude of a waveform displayed on an oscillogram, is virtually identical to the full wave value.

Probe Location	Without Arrestor Voltage(% of Line End)	With Arrestor Voltage(% of Line End)
Line End	100	35
18l	90	32
16l	71	22
14l	49	18
12l	34	12
12r	26	10
14r	22	7
16r	13	5
18r	9	2

where 18l means layer 8 left leg and 16r means layer 6 right leg et cetera

Table 11 Chopped Wave Layer-to-Ground Test Results

3.3.4 Chopped Wave Tests Layer To Layer

Table 12 shows the layer-to-layer voltages that were measured when a chopped waveform was applied to the line end terminals. As expected the values measured were slightly lower than those obtained without the arrestor in place. Also the location of maximum value shifted; being between layers six and four of the left leg coil. Without the arrestor this value was 24 percent or 22.8 kilovolts; however, with an arrestor the value decreased to 10 percent or 9.5 kilovolts. Again the difference between the location and value of the maximum voltage for a full wave and chopped impulse is due to the different waveform frequency components.

Probe Location	Without Arrestor Voltage(% of Line End)	With Arrestor Voltage(% of Line End)
line-18l	10	8
18l-16l	18	8
16l-14l	24	10
14l-12l	18	8
12l-12r	18	7
12r-14r	11	6
14r-16r	10	2
16r-18r	12	2

where 18l means layer 8 left leg and 16r means layer 6 right leg et cetera

Table 12 Chopped Wave Layer-to-Layer Test Results

By observing Figure 39 which is a plot of Tables 11 and 12 and comparing it to Figure 26, the more pronounced reduction of voltage with respect to position in the winding is highlighted. The circles and triangles and the full and dashed lines are associated with line-to-ground and layer-to-layer voltages respectively. Also the slight variations of the layer-to-layer voltages can be observed. A straight line voltage distribution is again drawn to illustrate the increasing non-linearity of the line-to-ground voltage distribution.

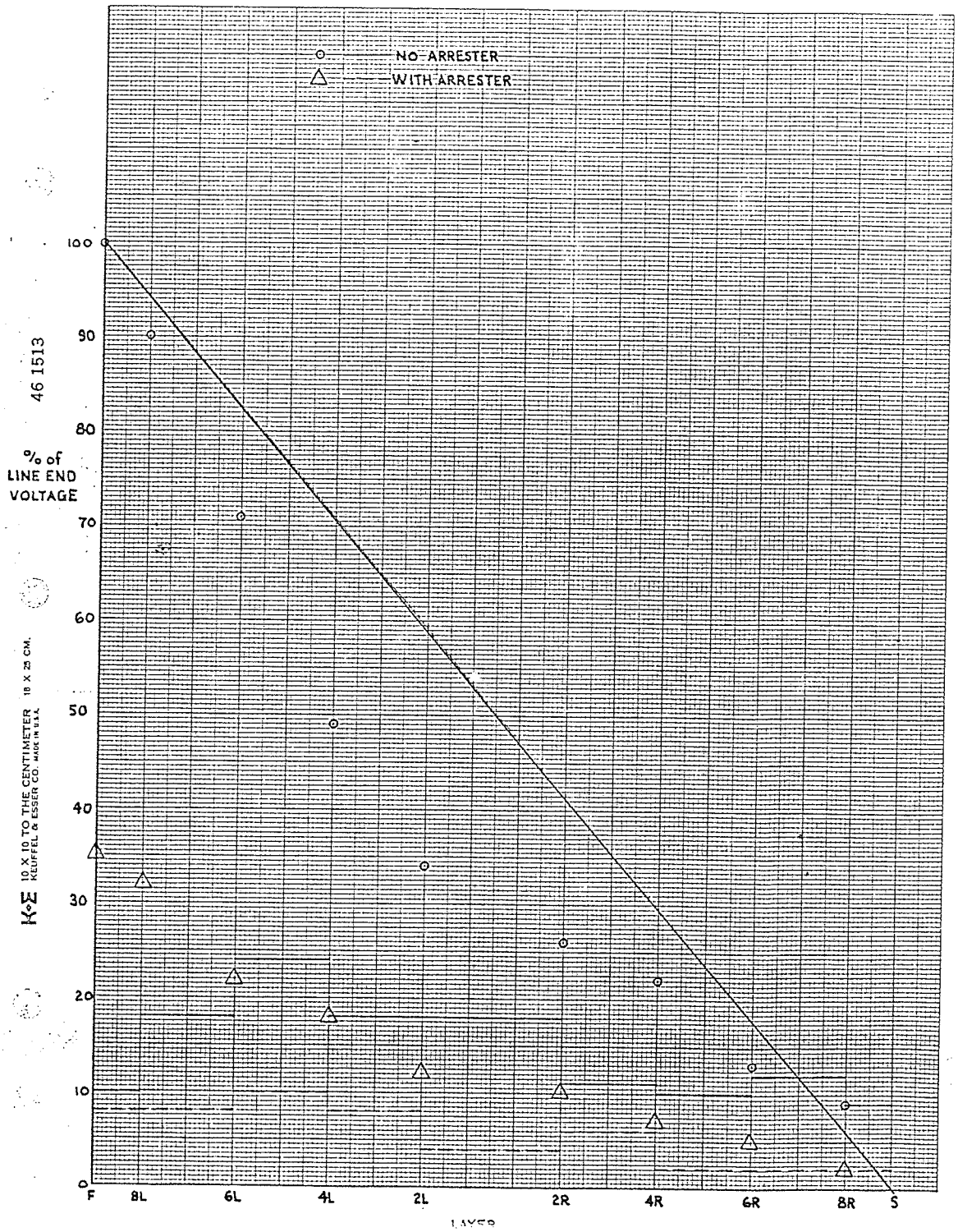

Figure 39 Chopped Wave Voltage Distribution in a Transformer Winding

Figures 40 to 51 are various oscillograms of the voltage waveforms produced by the chopped impulse wave. The line-to-ground and line-to-line voltages are shown alternately for each of the two cases; that is the transformer with and without the arrestor. The ringing once the voltage is chopped to zero, is due to the various inductance capacitance combination in the leads and transformer itself. It is interesting to note that although the impulse wave is chopped at three microseconds the voltage across the arrestor continues for approximately fifteen microseconds. The main reason for this would appear due to the presence of the transformer in the circuit, which sustains the flow of current through the arrestor.

20% per
division

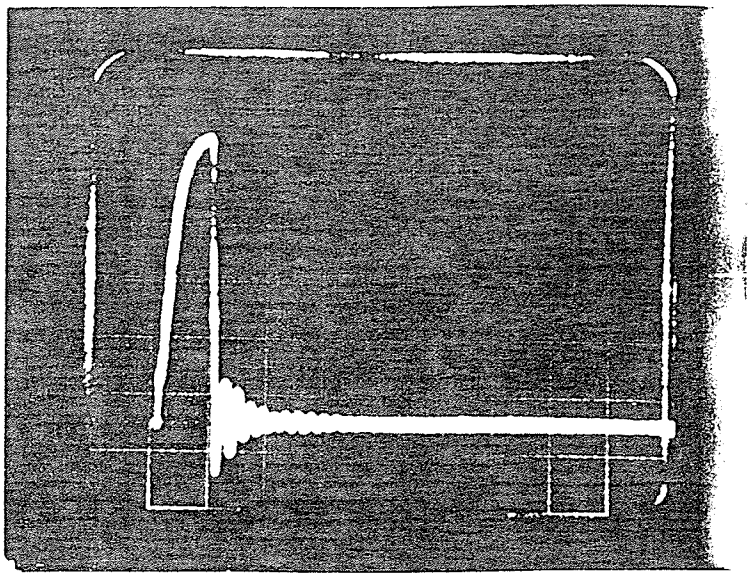

20 microseconds/division

Figure 40 Line-to-Ground Voltage No Arrestor

20% per
division

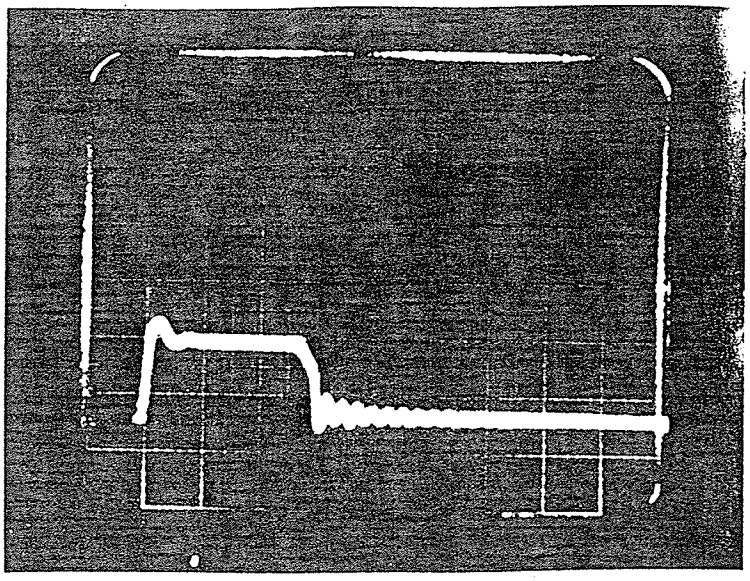

20 microseconds/division

Figure 41 Line-to-Ground Voltage With Arrestor

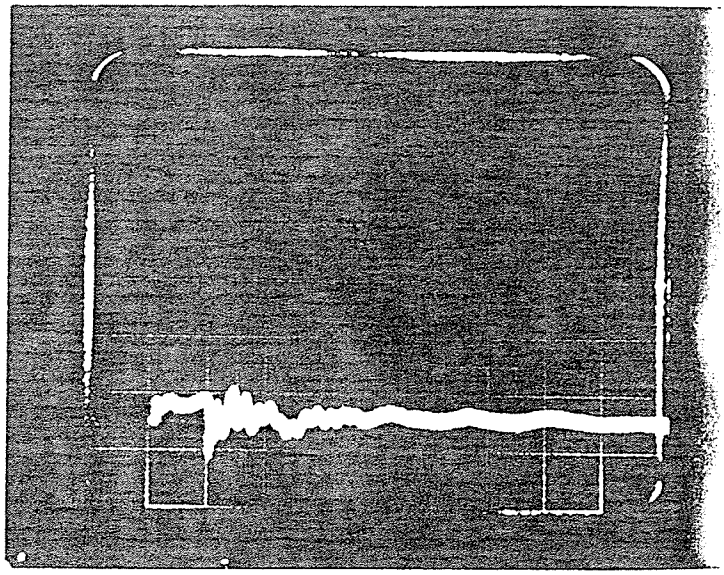

20% per division

20 microseconds/division

Figure 42 Layer 2, Left Leg-to-Ground Voltage No Arrestor

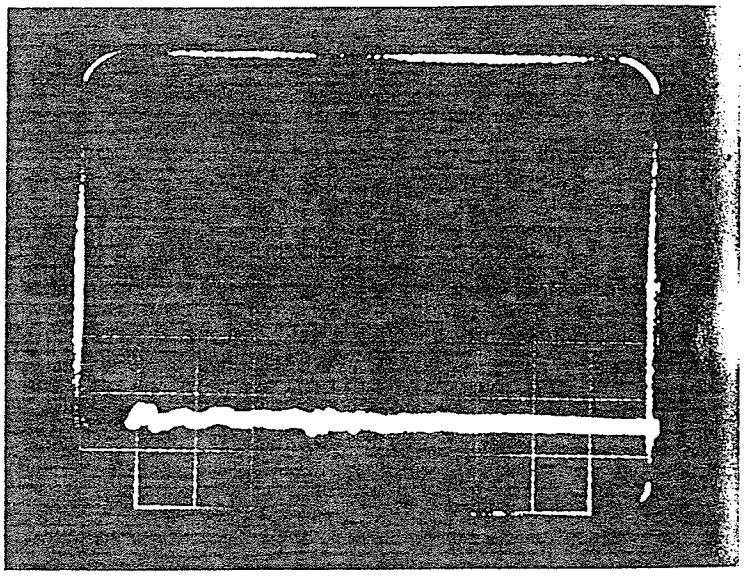

20% per division

20 microseconds/division

Figure 43 Layer 2, Left Leg-to-Ground Voltage With Arrestor

20% per
division

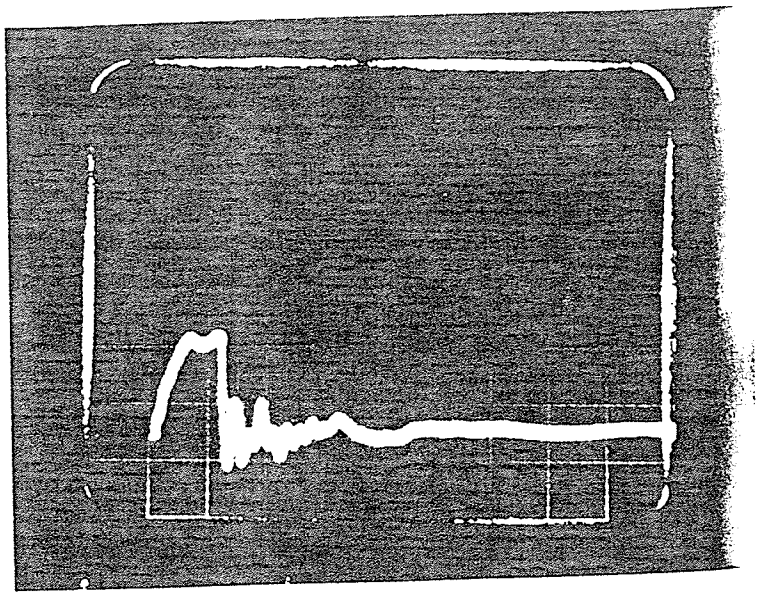

20 microseconds/division

Figure 44 Layer 6, Right Leg-to-Ground Voltage No Arrestor

20% per
division

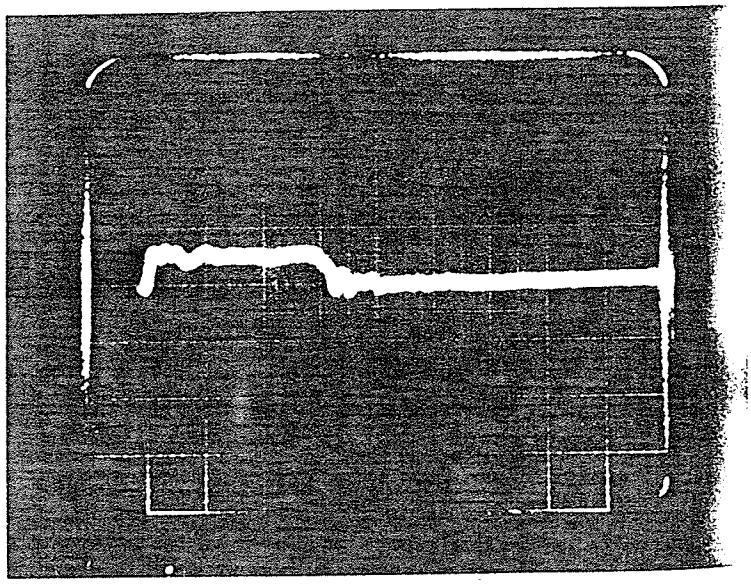

20 microseconds/division

Figure 45 Layer 6, Right Leg-to-Ground Voltage With Arrestor

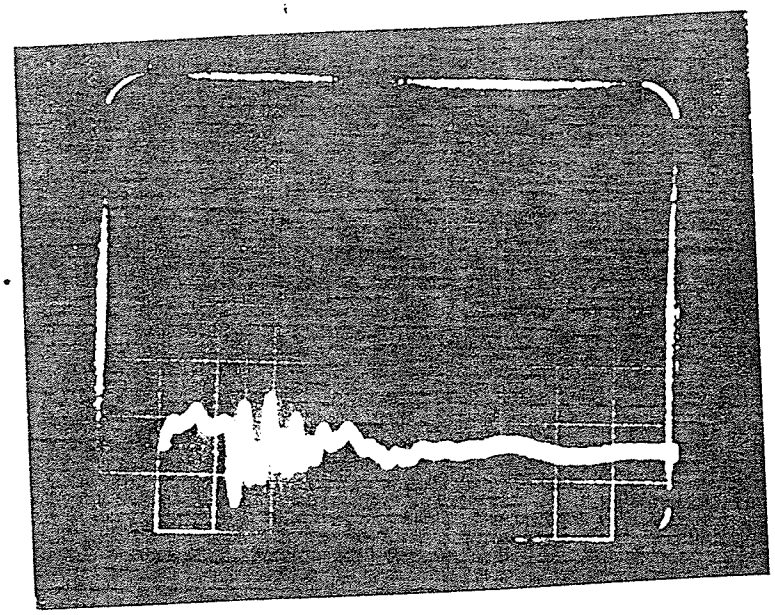

20% per division

20 microseconds/division

Figure 46 Line-to-Layer 8, Left Leg Voltage No Arrestor

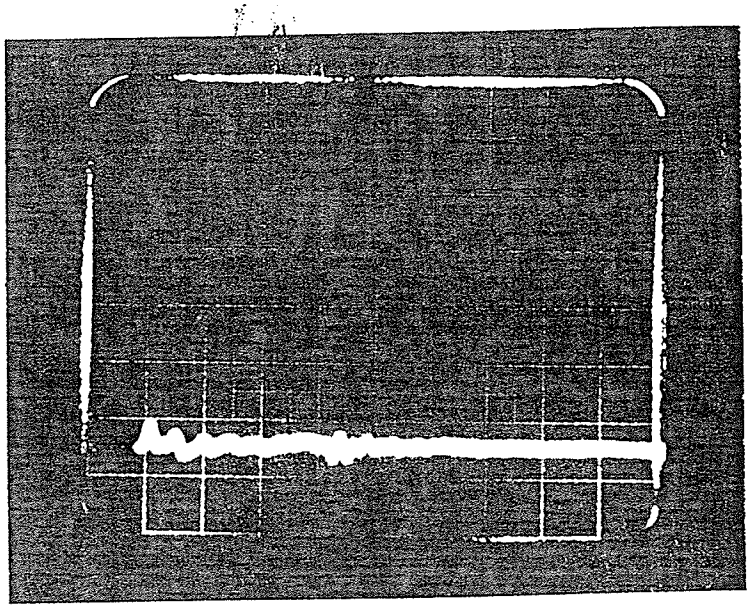

20% per division

20 microseconds/division

Figure 47 Line-to-Layer 8, Right Leg Voltage With Arrestor

20% per division

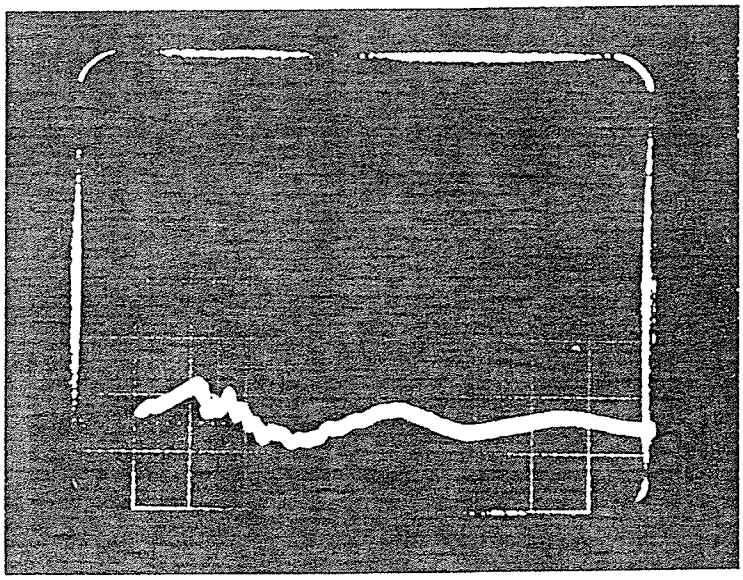

20 microseconds/division

Figure 48 Layer 2, Left Leg-to-Layer 2, Right Leg Voltage No Arrestor

20% per division

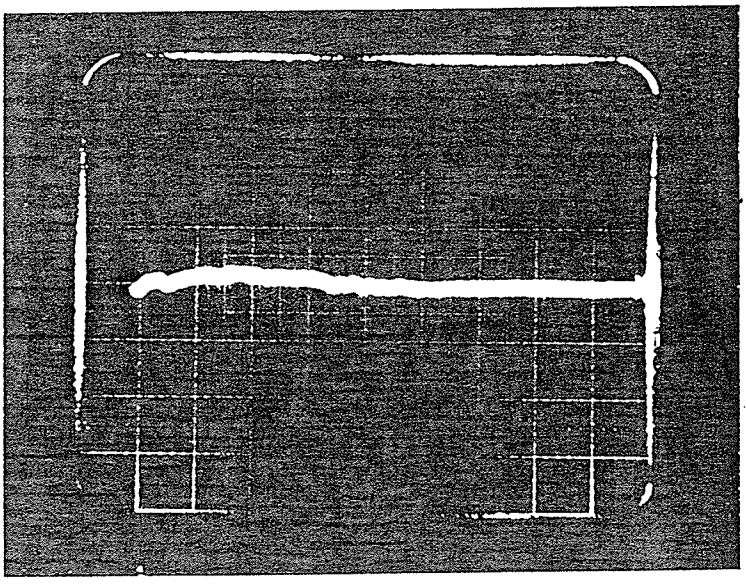

20 microseconds/division

Figure 49 Layer 2, Left Leg-to-Layer 2, Right Leg Voltage With Arrestor

20% per division

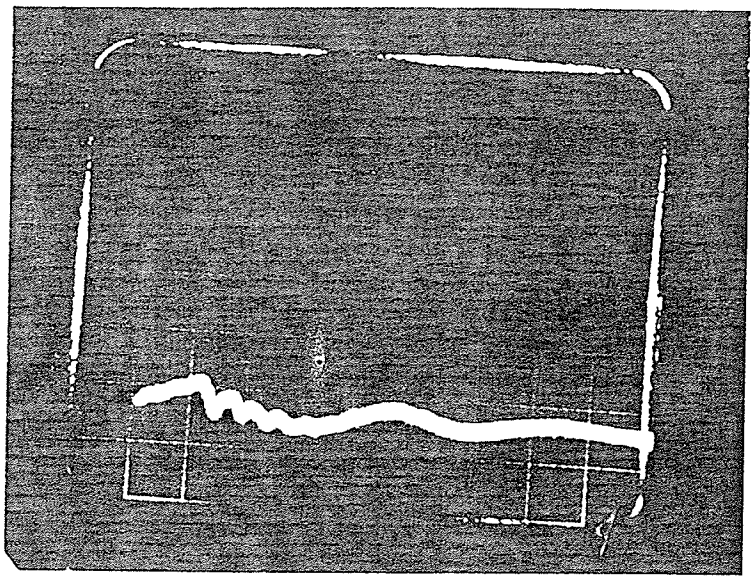

20 microseconds/division

Figure 50 Layer 6, Right Leg-to-Layer 8, Right Leg Voltage No Arrestor

20% per division

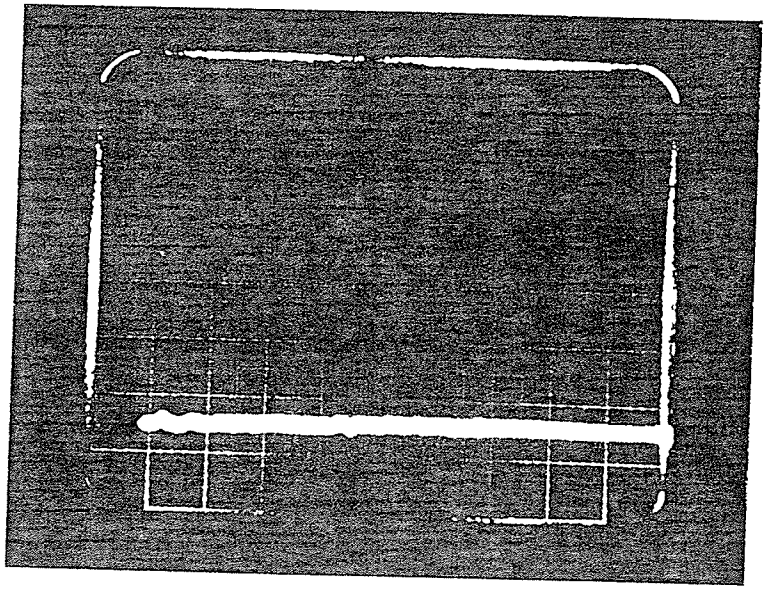

20 microseconds/division

Figure 51 Layer 6, Right Leg-to-Layer 8, Right Leg Voltage With Arrestor

3.4 Actual Impulse Tests

An impulse voltage test was performed on an actual transformer. The test was performed with and without the arrestor in place. Figures 52 to 56, which are the oscillograms from the test, show the full wave voltage, the transformer current, the voltage waveform with the arrestor, and the transformer and arrestor currents. Comparing Figure 52 to Figure 27 it is apparent that the RSG waveform is essentially the same as the 95 kilovolt impulse waveform. The RSG voltage waveform with the arrestor, Figure 28, is quite similar to Figure 54, the actual arrestor voltage waveform. Some of the differences are due to the slight differences in waveshapes, 1 x 45 microseconds and 1.25 x 53 microseconds for the RSG and actual test respectively. As well the physical difference between the arrestors used in both tests played a large role in the respective waveshapes. For the RSG test the arrestor was very small while the actual arrestor components were three cylindrical blocks 1.625 inches in diameter. Also different oscilloscopes were employed in both cases, with different inductance and capacitance values in the associated measuring circuitry. However, it is believed that the RSG results are indeed representative of what actually occurs at the full scale voltage.

3.47 kilovolts
per millimeter

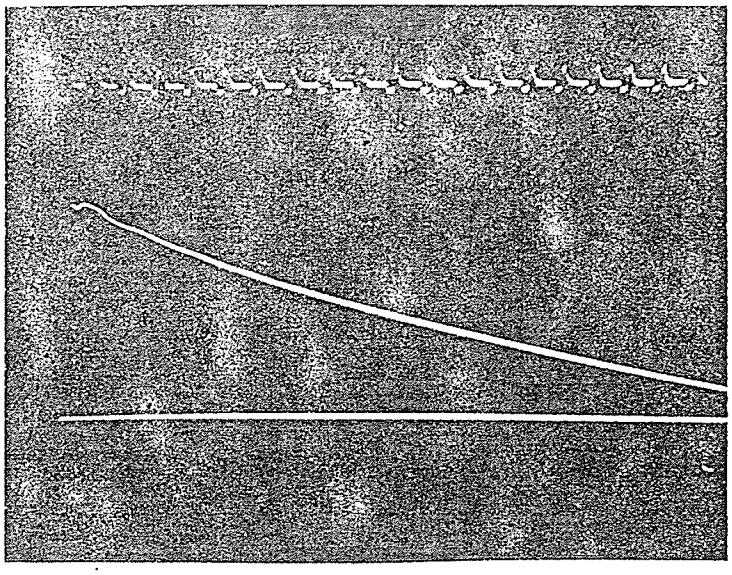

1.15 microseconds per millimeter

Figure 52 95 kV Full Wave Impulse Waveform No Arrestor

1790 amps
per centimeter

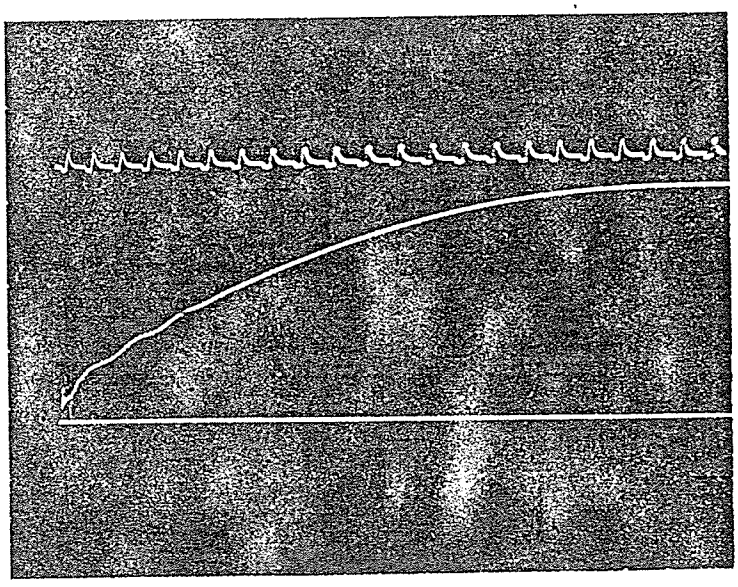

1.15 microseconds per millimeter

Figure 53 Transformer Current No Arrestor

3.47 kilovolts
per millimeter

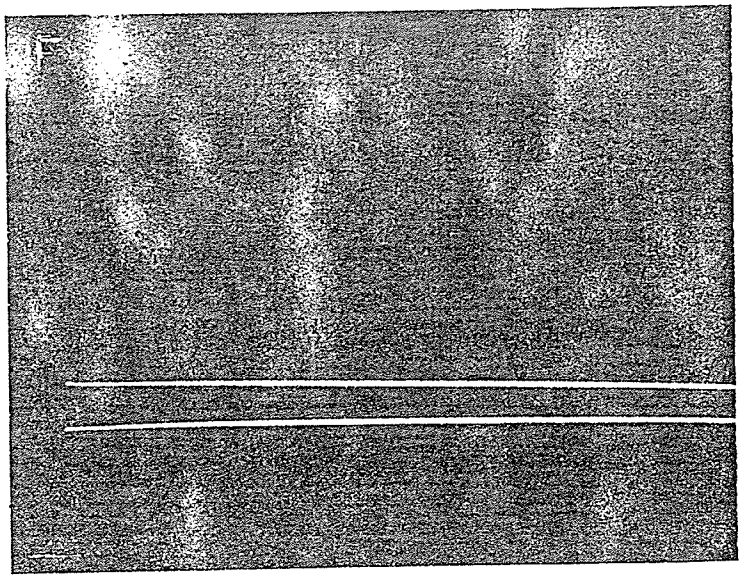

1.15 microseconds per millimeter

Figure 54 Voltage Waveform With Arrestor

2237.5 amps
per centimeter

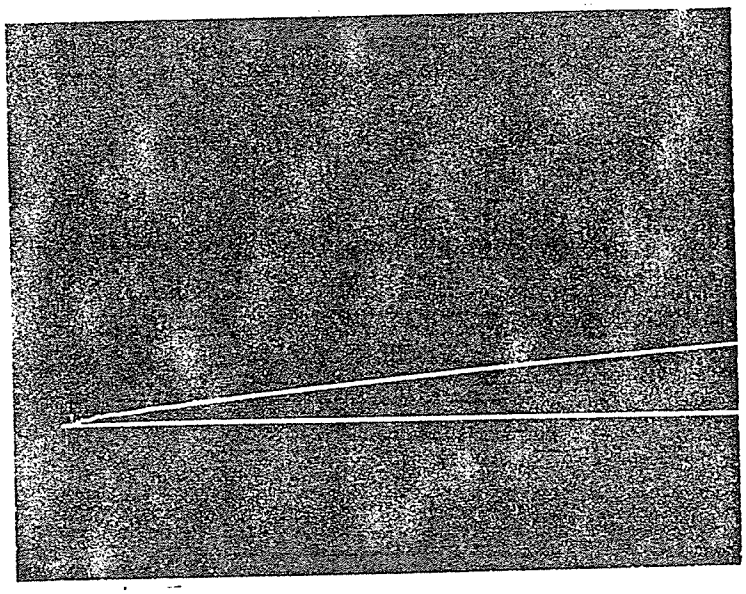

1.15 microseconds per millimeter

Figure 55 Transformer Current With Arrestor

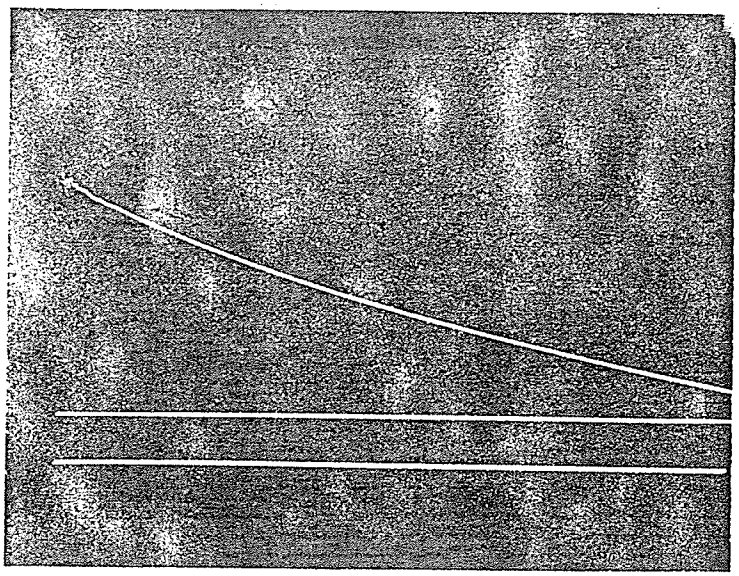

Figure 56 Current Through the Arrestor

3.4.1 Energy Conservation

The energy balance in the transformer-arrestor assembly was verified by using Equation 3. Initially the value of 2.542 kilojoules was found by graphically multiplying Figures 52 and 53 and summing the area under the curve. Next the same process was performed with Figures 54 and 55, the arrestor voltage and transformer current, and Figures 54 and 56, the arrestor voltage and current. The energy values were found to be 514.8 joules and 2.048 kilojoules respectively; the sum of which is 2.5628 kilojoules. After taking reading errors into account the law of conservation of energy is preserved. It is interesting to note

that the arrestor absorbs 80 percent of the total energy available in the simulated lightning stroke. However, one manufacturer rates its arrestor at 200 joules per cubic centimeter; therefore, a typical 9 kilovolt class arrestor can safely dissipated 14 kilojoules, which is well above the tested levels. The 10 kiloamp current and corresponding discharge voltage used in the standard protective margin calculation produces approximately 6.3 kilojoules which is also well below the arrestors limit.

3.5 Transformer Design

Having performed all the tests on the transformer-arrestor assembly it is now possible to design a transformer with the reduced insulation levels. Due to proprietary reasons actual prices are not discussed, but rather the costs are expressed in percentages with respect to a standard 25 KVA, single phase, 7200-120/240 volt, no taps, 65 degree celsius, pole type transformer without internal overvoltage protection. Table 13 illustrates the major changes and the associated reduction in costs for a 25 KVA pole type transformer. The major costs in this type of distribution transformer are the tank, insulating oil, coils and cores. It can be seen that a transformer with reduced insulation levels but without an arrestor has a final cost which is 86.33 percent of the standard unit. Comparing component costs in the standard design and the design with

reduced insulation, it is seen that the tank, oil, coils and core costs in the latter case are 69.55 percent, 61.10 percent, 79.52 percent and 100 percent respectively of the corresponding costs in the standard design. A further reduction in price would be possible if the core window size can be decreased. However, further work is required to determine if this is possible for all units irrespective of the voltage class. With the addition of the arrestor, whose cost is 26.12 percent, the final cost for this specific transformer with internal over voltage protection and reduced insulation is 112.45 percent. This cost, however, does not reflect the advantages of this type of unit with its inherently greater reliability than a conventional transformer. Depending upon the application, a utility may be more concerned with system protection than unit cost. Therefore, the under-oil arrestor may be installed within a standard transformer.

25 kVA Pole Type Transformer

	Standard Design	Design with Reduced Insulation
Tank	7.16%	4.98%
Insulating Oil	16.30%	9.96%
Coils	25.15%	20.00%
Core	29.47%	29.47%
Others	21.97%	21.92%
Total	100.00%	86.33%
Total with Arrestor		112.45%

Table 13 Cost Comparison

4. Conclusions and Recommendations

1) Thermal tests reported and conducted by the various under oil-arrestor manufacturers and undertaken during the course of this thesis have indicated that the Zinc Oxide blocks are unaffected by oil immersion.

2) By placing the arrestor inside the tank under oil many problems with externally mounted arrestors have been eliminated and the arrestor-transformer system reliability has been improved.

3) Recurrent Surge Generator tests have shown internal over voltage protection to be viable means of limiting voltage levels within a transformer's coils.

4) The installation of an under-oil arrestor provides cost savings, neglecting the cost of arrestor, in the form of reduced clearances and reduced voltage stresses within the transformer coils.

5) Although under-oil arrestors have eliminated many problems that are associated with externally mounted lightning arrestors, the most suitable applications for this technology are in underground distribution and environments with salt spray or high contamination.

References

1) D. S. Smith, "Study of Distribution Transformer Failures with Special Reference to 25kV", C.E.A. Research Report, C.E.A. Contract No. 75-11, September 1977

2) American National Standards Institute, "Guide for the Application of Valve-Type Surge Arrestors for Alternating Current Systems", ANSI C62.2, 1981

3) American National Standards Institute, "Guide for Loading Mineral Oil Immersed Overhead Type Distribution Transformers With 55°C. or 65°C. Average Winding Rise", ANSI C57.91, 1981

4) American National Standards Institute, "Standard for Metal Oxide Surge Arrestors for Alternating Current Systems", Proposed ANSI C62.11, Draft 6, October 1985

5) M. Kobayashi, M. Minzuno, et al., "Development of Zinc Oxide Non-Linear Resistors and Their Application to Gapless Surge Arrestors", IEEE Transactions On Power Systems & Apparatus, Vol. PAS-97, No. 4, p. 1149-58, July-August 1978

6) J. J. Lee, M.S. Cooper, "High Energy Solid State Electrical Surge Arrestor" ,IEEE Transactions on Parts, Hybrids and Packaging, Vol. PHP-13, No.4, p. 413-19,December 1977

7) P. R. Emtage, "The Physics of Zinc Oxide Varistors", Journal of Applied Physics, Vol. 48, No. 10, October 1977

8) S. Tominaga, K.Azumi, et al., "Protective Performance of Metal Oxide Surge Arrestor Based Upon the Dynamic V-I Characteristics", IEEE Transactions on Power Apparatus and Systems, Vol. PAS-98, No. 6, p. 1860-71, Nov/Dec 1979

9) M. Oyama, I. Ohshima, et al., "Analytical and Experimental Approach to the Voltage Distribution on Gapless Zinc Oxide Surge Arrestors", IEEE Transactions on Power Apparatus and Systems, Vol. PAS-100, No. 11, p. 4621-7, Nov 1981

10) D. B. Miller, R. W. Reuther, et al., "Development of Gapless Metal Oxide Surge Arrestor for 362kV Gas Insulated Substations", IEEE Transactions on Power Apparatus and Systems, Vol. PAS-101, No. 7, p. 2178-86, July 1982

11) M. E. Potter, T. O. Sokoly, "Development of Metal Oxide Varistors for Gas-Insulated Surge Arrestors", IEEE Transactions on Power Apparatus and Systems, Vol. PAS-101, No. 7, p. 2217-20, July 1982

12) W. D. Niebuhr, "Application of Metal Oxide-Varistor Surge Arrestor on Distribution Systems", IEEE Transactions on Power Apparatus and Systems, Vol. PAS-101, No. 6, p.1711-15, June 1982

13) R. J. Bronikowski, J. DuPont, "Development and Testing of Move Arrestor Elements", IEEE Transactions on Power Apparatus and Systems, Vol. PAS-101, No. 6, p. 1638-42, June 1982

14) W. D. Niebuhr, "Protection of Underground Distribution Systems Using Metal Oxide Surge Arrestors", IEEE Transactions on Industry Applications, Vol. IA-18, No. 2, p. 1095-1104, May 1982

15) E. C. Sakshaug, J. S. Kresge, S. A. Miske Jr., "A New Concept in Station Arrestor Design", IEEE Transactions on Power Apparatus and Systems, Vol. PAS-96, No. 2, p. 647-56, 1977

16) M. Oyama, I. Ohshima, et al., "Life Performance of Zinc Oxide Elements Under DC Voltage", IEEE Transactions on Power Apparatus and Systems, Vol. PAS-101, Zinc Oxide Elements Under DC Voltage", IEEE Transactions on Power Apparatus and Systems, Vol. PAS-101, No.6, p. 1363-8, June 1982

17) U. Burger, "Insulation Coordination and Selection of Surge Arrestor", Brown Boveri Review, Switzerland, Vol. 66, No. 4, p. 271-80, April 1979

18) S. Tominaga, K. Azumi, et al., "Reliability and Application of Metal Oxide Surge Arrestors for Power Systems", IEEE Transactions on Power Apparatus and Systems, Vol. PAS-98, No. 3, p. 805-16, May/June 1979

19) S. Tominaga, T. Shibuya, et al., "Stability and Long Term Degradation of Metal Oxide Surge Arrestors", IEEE Transactions on Power Apparatus and Systems, Vol. PAS-99, No. 4, p. 1548-56, July/August 1980

20) U. Burger, B. Knecht, "Surge Arrestors: Conventional Technology- Metal Oxide Resistors", Brown Boveri Review, Switzerland, Vol. 66, No. 11, p. 734-8, November 1979

21) M. Kan, S. Nishiwaki, et al., "Surge Discharge Capability and Thermal Stability of a Metal Oxide Surge Arrestor", IEEE Transactions on Power Apparatus and Systems, Vol. PAS-102, No. 2, p. 282-9, February 1983

22) A. Mizukoshi, J. Ozawa, et al., "Influence of Uniformity on Energy Absorption Capabilities of Zinc Oxide Elements as Applied in Arrestors", IEEE Transactions on Power Apparatus and Systems, Vol. PAS-102, No. 5, p. 1384-90, May 1983

23) M. V. Lat, "Thermal Properties of Metal Oxide Surge Arrestors", IEEE Transactions on Power Apparatus and Systems, Vol. PAS-102, No. 7, p. 2194-202, July 1983

24) G. St-Jean, Y. Latour, "Comparison of the Capabilities of Metal Oxide and Conventional HV Surge Arrestors", Electric Power Systems Research, Switzerland, Vol. 7, No. 1, p.45-52, January 1984

25) C. J. McMillen, M. G. Comber, et al.,"The Development of an Oil-Immersed Surge Arrestor for Distribution Transformers", IEEE Transactions on Power Apparatus and Systems, Vol. PAS-180, No. 5, p. 2492-2500, September 1985

26) J. B. Posey, "Under-Oil Arrestors in Transformer Tanks", Southeastern Electric Exchange, Distribution Section, Sea Coast Area Distribution System Conference, Wrightsville Beach, North Carolina, Paper EU1090-H, June 10-12, 1985

27) J. B. Wisniewski, C. Chatterji, "Metal Oxide Arrestors-Their Characteristics and Application in Power Systems", Transmission and Substation Conference, Chicago, Illinois, Paper T&S-P36, November 13, 1980

28) General Electric Company, "Surge Characteristics and Protection of Distribution Transformers", Electric Power Research Institute Project 1532-1, EPRI EL-3385, Final Report, January 1984

29) D. W. Lenk, "An Examination of the Pollution Performance of Gapped and Gapless Metal Oxide Surge Arrestors", IEEE Transactions on Power Apparatus and Systems, Vol. PAS-103, No. 2, p.337-44, February 1984

30) S. Nishiwaki, H. Kimura, et al., "Study of Thermal Runaway/Equivalent Prorated Model of a Zinc Oxide Surge Arrestor", IEEE Transactions on Power Apparatus and Systems, Vol. PAS-103, No. 2, p. 413-21, February 1984

31) Ohio Brass Company, "Seminar Notes", MOV Surge Arrestor Seminar, Akron Ohio, October 22-23, 1985

32) Canadian Standards Association, "Insulating Oil, Electrical For Transformers and Switches", CSA C50-1976

33) F. A. Goba, "Bibliography on Thermal Aging of Electrical Insulation", IEEE Transactions on Electrical Insulation, Vol. EI-4, No. 2, June 1969

Appendix 1 Physics of Zinc Oxide Blocks

Since this thesis is application oriented, a more theoretical description of ZnO blocks may be found in the references listed in the reference section.[7][31] The insulation layer between ZnO grains is responsible for the varistor type of behavior. This oxide layer is approximately 20 angstroms thick (1 angstrom= $1x10^{-10}$ meters) however high frequency capacitance measurements have shown this boundary to be 1000 angstroms thick. This is because the boundary layer extends into the ZnO grains, which requires the formation of space charge layers in the ZnO grains; that is layers which are depleted of free carriers. It is possible to achieve this by doping the intergranular layer with oxides possessing a high density of traps, oxide molecules with a net positive charge. By adding the boundaries in series along a single current path and then summing the parallel paths, the electrical response of a varistor may be determined. A model of two back-to-back Schottky barriers at each interface provides a reasonable explanation of the variation of the volt-ampere characteristic and dielectric properties of the varistor.

There are essentially three distinct zones: a low, intermediate and high voltage zone. At low voltages the insulating barrier absorbs the free electrons; this results in very low and almost ohmic conduction. As the voltage is increased

further, the current increases dramatically. The current can increase five or six orders of magnitude while the voltage changes only by 50 percent. In this portion of the volt-ampere characteristics the exponent in Equation 2 varies between 30 and 40. Once the current density increases substantially the voltage again starts to increase. The increase is linear and associated with the resistance of the ZnO grains.

Appendix 2 Manufacturing of Zinc Oxide Blocks

Although Matsushita licenses the technology to every ZnO arrestor manufacturer, each has its own proprietary mix and variation of design steps. The blocks are approximately 90 percent ZnO by weight with the remaining portion being made up of Bi_2O_3, Sb_2O_3, Cr_2O_3, NiO, MgO, CaO, TiO_2, Co_3O_4, MnO, SiO_2 et cetera all of which are initially in the powder form of 0.2 to 5.0 micrometers in diameter. The actual manufacturing process is as follows:[31]

-weigh the correct amounts of oxide additives except for ZnO

-ball mill the additives

-calcine the additives to pre-react the oxides

-ball mill the calcined product to mix and reduce the particle size

-mix the calcined material with required amount of ZnO

-spray dry the slurry to form a pressable powder

-press the pucks

-burn out the organic binder

-sinter

-lap the block faces

-apply and cure an insulation collar and electrodes

-electrically test and sort.

The proportion of additives must be carefully monitored since small changes in amounts can cause the volt-ampere

characteristics to be shifted left or right and up or down. As well the exponent b in Equation 2 can be affected.

Appendix 3 Arrhenius Plots

The plot of arrestor life versus operation temperature is based on the well known Arrhenius equation, for chemical reaction rates.

$$\text{Rate} = A_c e^{-E/RT} = A_c e^{-B_c/T} \quad \text{in time}$$

where E= activation energy for the reaction

R= the gas constant per gram molecule weight

B_c= a constant from combining E & R

This can be rearranged to give the following equation

$$\ln(L)=\ln(A_c)+B_c/T$$

where L= life of the assembly to a given test point

Usually this equation is plotted on semi-logarithmic paper to give a linear graph. By conducting tests at high temperatures, which result in short test intervals, several points on the may be obtained. The graph is then extrapolated or interpolated to give a life expectancy at the actual operating conditions.

The test procedures are based upon certain criteria such as the point in time at which the watts measured are double the initial measured value as in the case of Zinc Oxide blocks. As well strict test procedures must be observed to ensure reliable results. A complete bibliography on thermal ageing, test procedures and applicable standards has been written by F. A. Goba entitled "Bibliography on Thermal Aging of Electrical Insulation".[33]

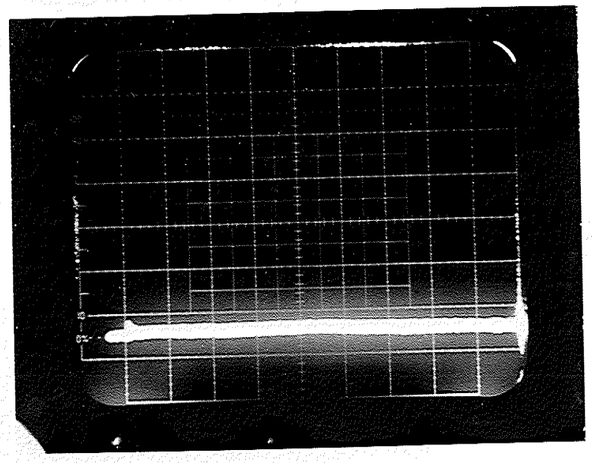

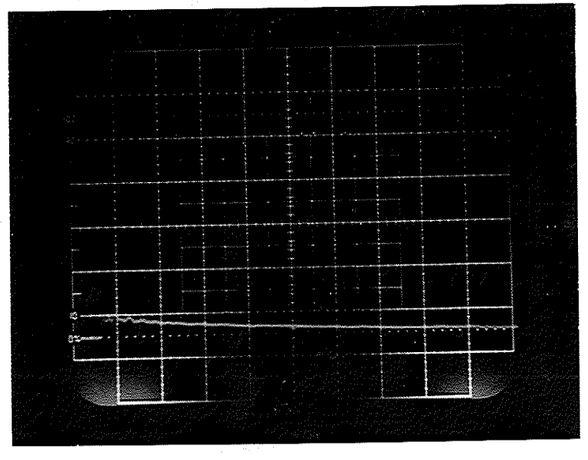

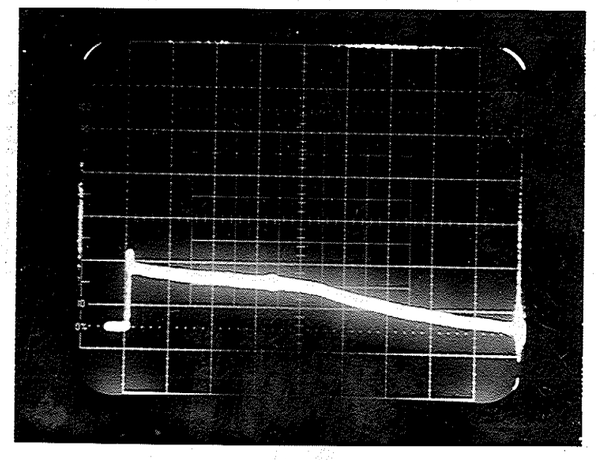

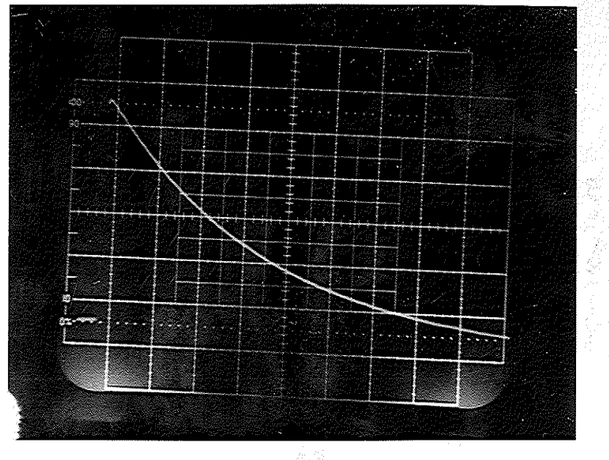

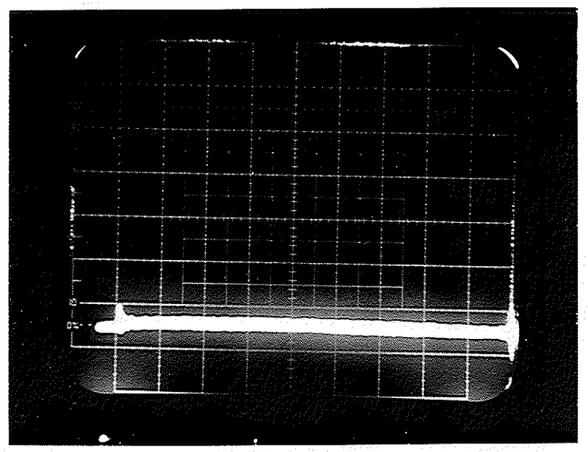

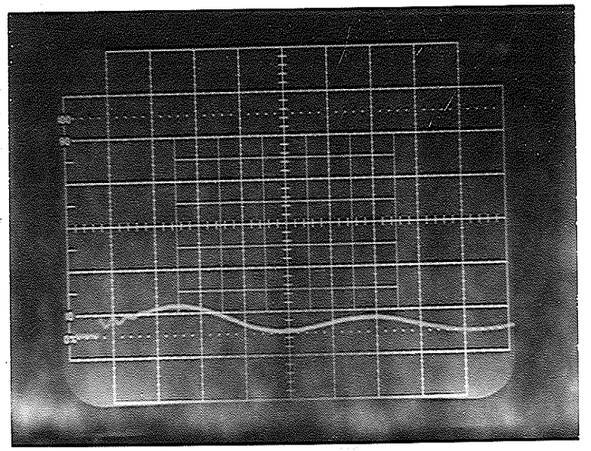

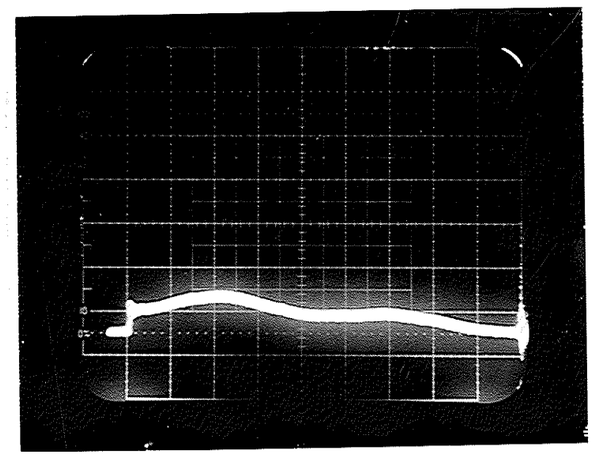

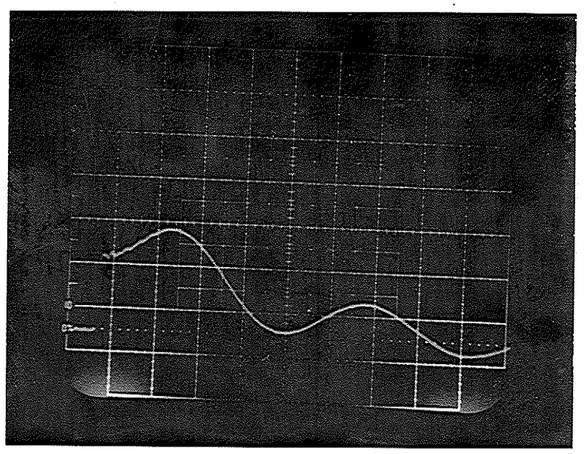

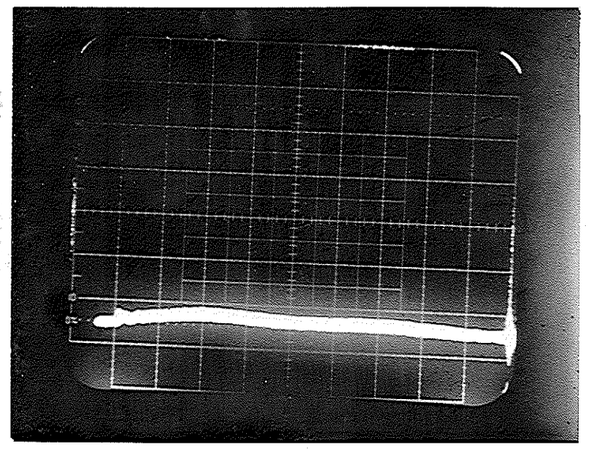

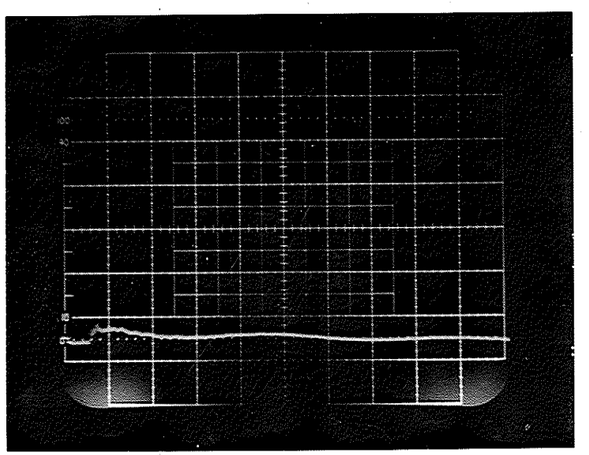

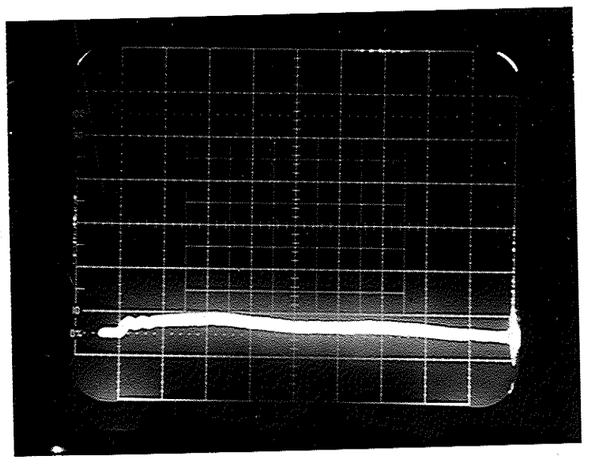

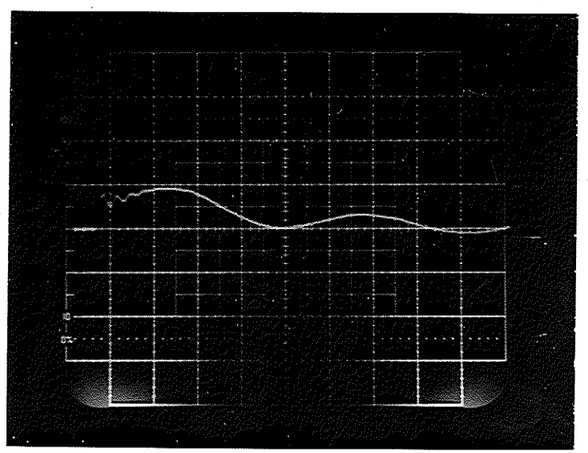

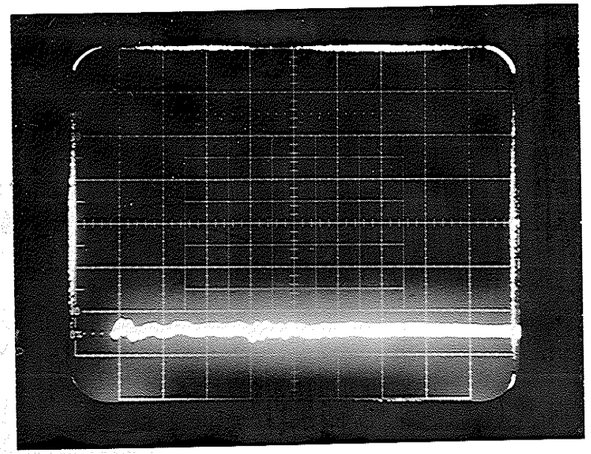

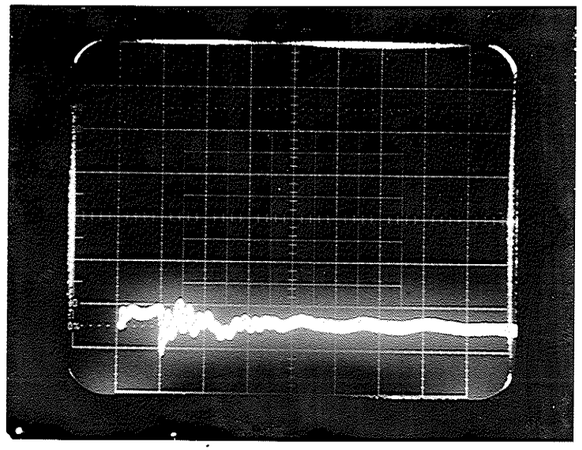

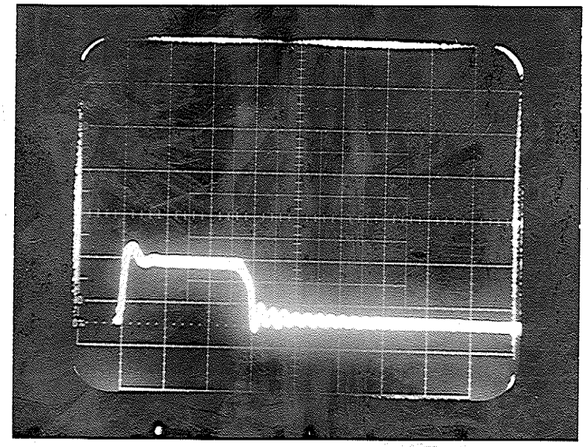

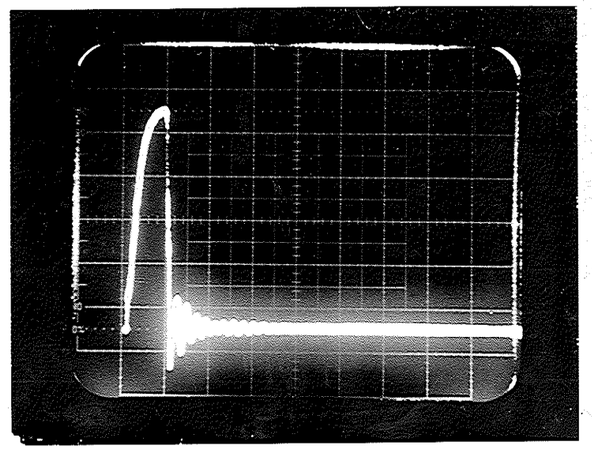

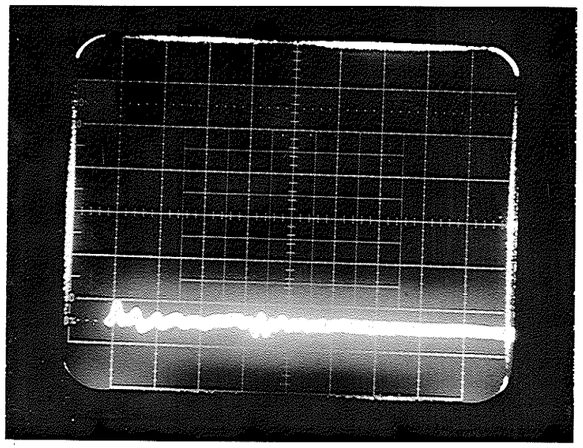

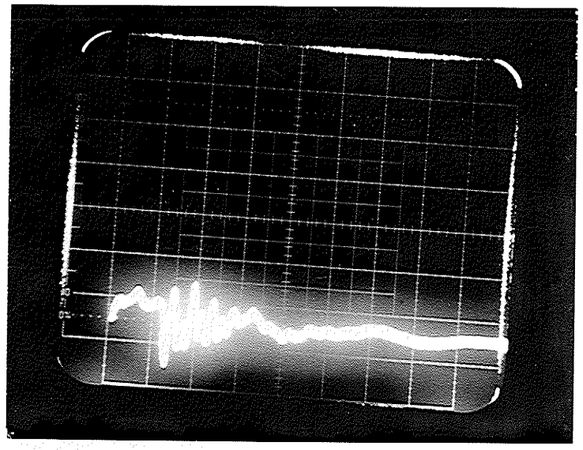

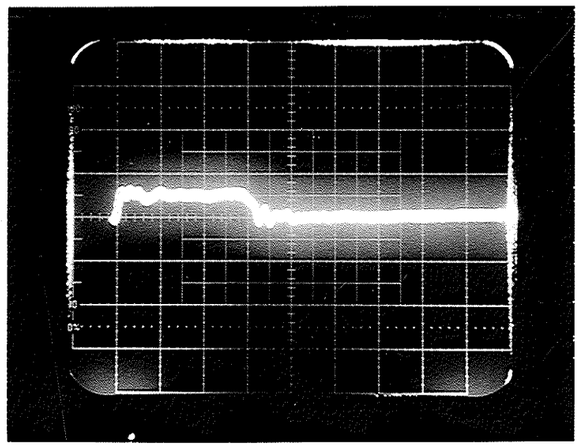

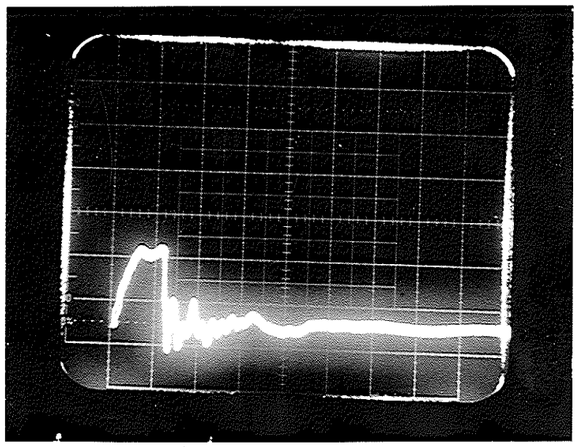

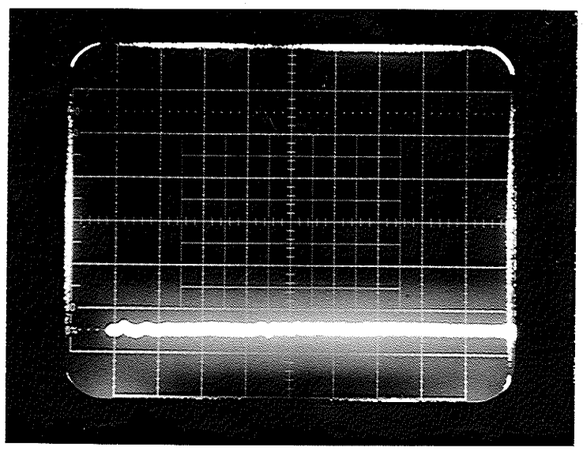

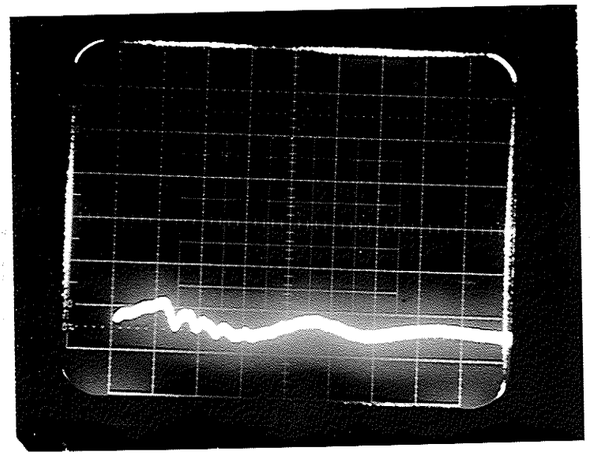

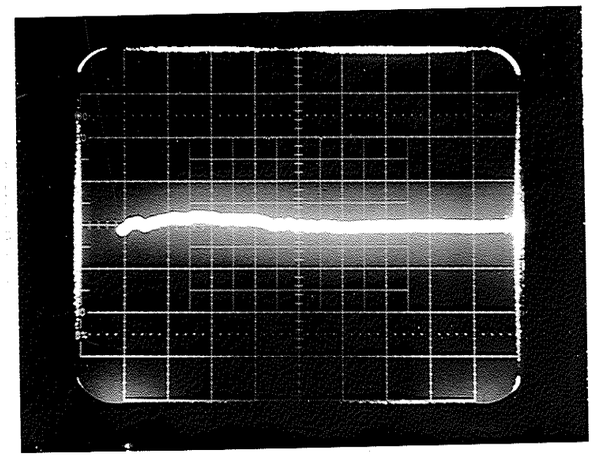

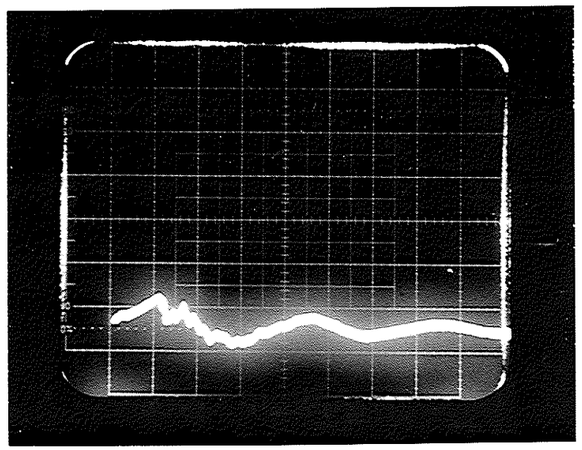

FW Current Through X former with Arrest

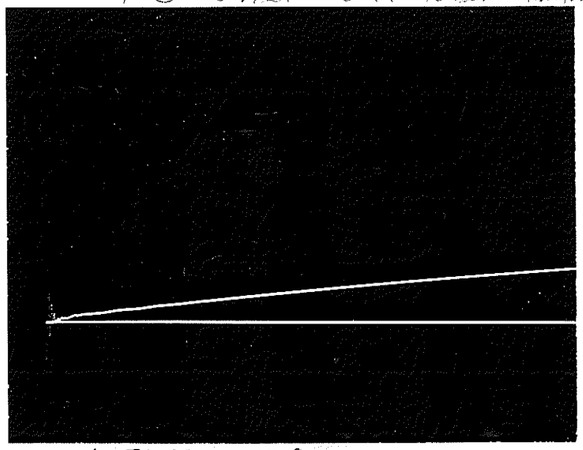

40% ATTENUATOR

FW 97.2 KV VOLTAGE NO ARRESTOR

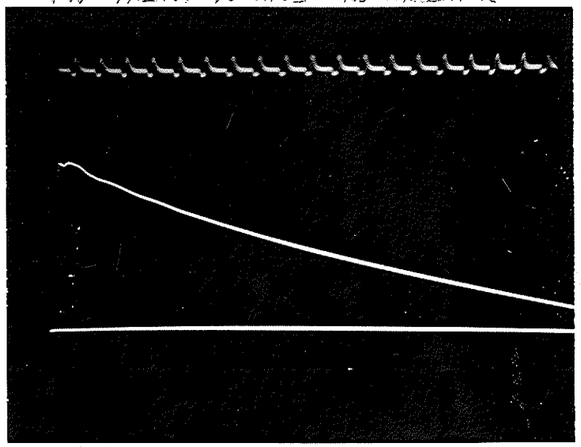

20% ATTENUATOR

FW Voltage With Arrestor

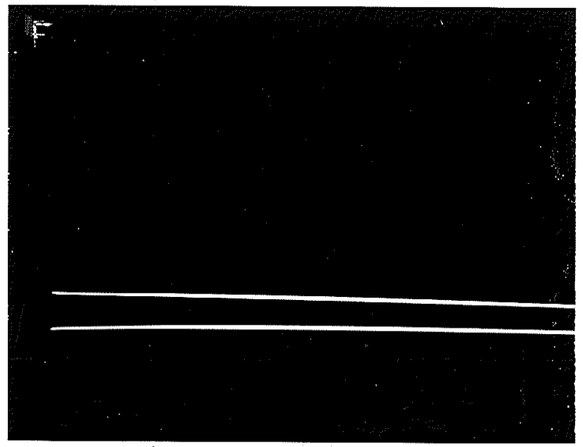

20% ATTENUATOR

FW CURRENT THROUGH ARRESTOR TRANSF IN

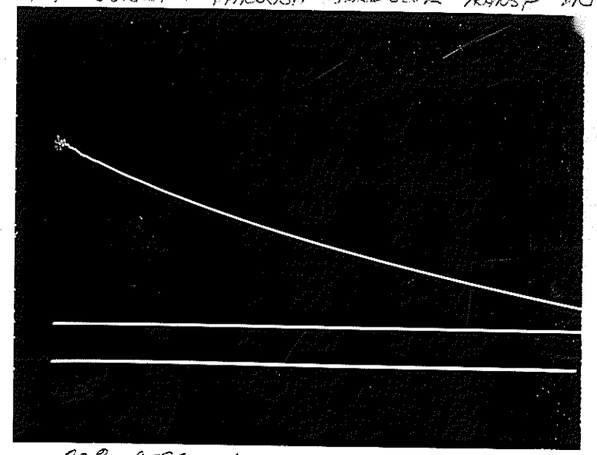

20% ATTENUATOR

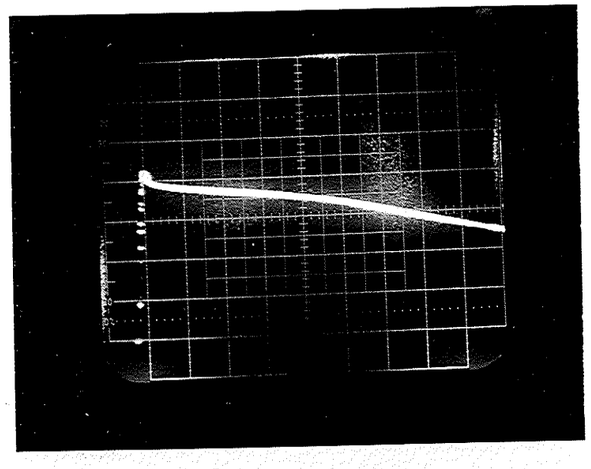

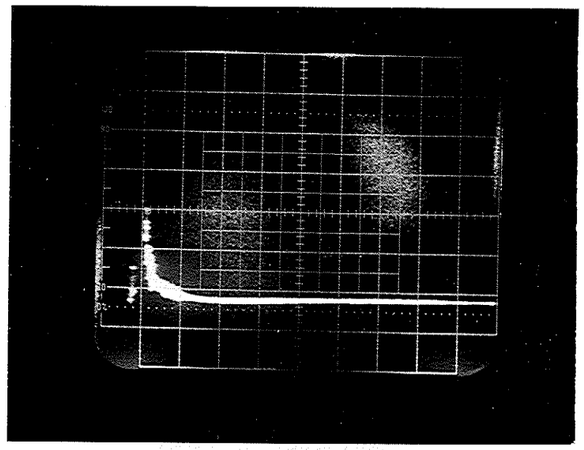

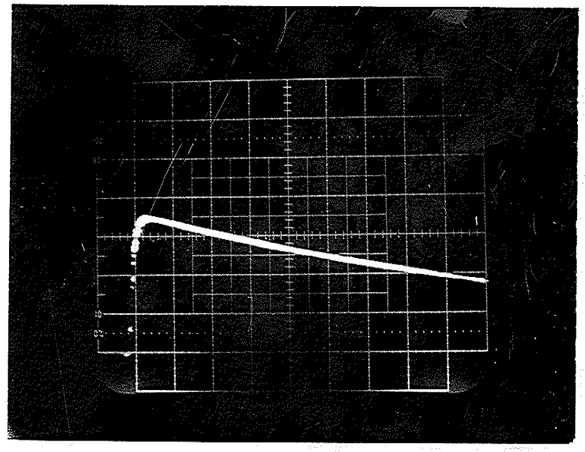

FW CURRENT NO ARRESTOR

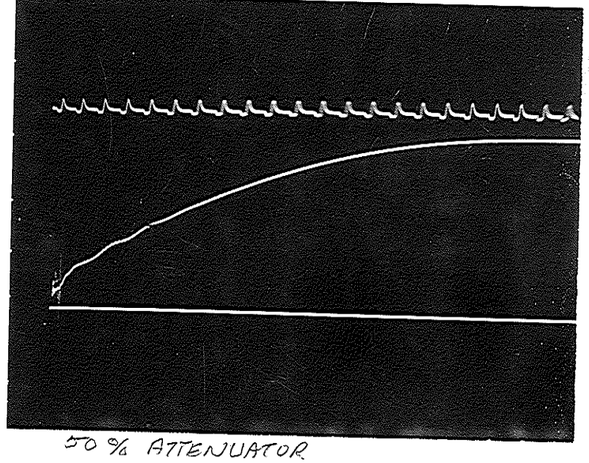

50% ATTENUATOR